Materials Chemistry and Physics 197 (2017) 163–180

Contents lists available at ScienceDirect

Materials Chemistry and Physics

journal homepage: www.elsevier.com/locate/matchemphys

Diffusion calculations with two atomic models in h.c.p Zr-Nb diluted alloys

Viviana P. Ramunni [a, b], Alejandro M.F. Rivas [a, c, *]

[a] CONiCET, Avda. Rivadavia 1917, CABA, C.P. 1033, Argentina
[b] Centro Atómico Constituyentes, Gerencia Materiales, Av. General Paz 1499, C.P. 1650, San Martín, Argentina
[c] Centro Atómico Constituyentes, Gerencia Física, Laboratorios Tandar, Av. General Paz 1499, C.P. 1650, San Martín, Argentina

HIGHLIGHTS

- Comparison of atomic diffusion multi-frequency models for h.c.p. lattices.
- Tests with three models, 13, 8 and 5-frequncy vacancy based diffusion models.
- Extensive computational analysis for dilute h.c.p Zr-Nb alloys is performed.
- Calculations with classical molecular techniques and ab-initio with LDA and GGA.
- Ab-initio calculations with 5-frequency model is sufficient for correct description.

ARTICLE INFO

Article history:
Received 7 July 2016
Received in revised form
2 March 2017
Accepted 12 May 2017
Available online 16 May 2017

Keywords:
Diluted alloys
Diffusion
Ab-initio calculations
Vacancy mechanism
$\alpha Zr - Nb$

ABSTRACT

In this work we perform a comparison of atomic diffusion multi-frequency models for h.c.p. lattices. Specifically, in diluted h.c.p. αZr-Nb alloy, we calculate, the tracer self- and impurity diffusion coefficients, with Ghate's eight frequencies model [1] and with the 13 frequencies model recently developed by Allnatt et al. [2]. For the latter we investigate the tight-binding limit and the 5-frequency limit of the model. Our exhaustive calculations have been performed using, for both models, classical molecular static techniques (MS), as well as, quantum ab-initio calculations within both LDA and GGA approximations. Our ab-initio calculations show that a, so called, 5-frequency model, without pairs dissociation nor anisotropy in the jump frequencies, that only needs three frequencies, is sufficient to obtain solvent and solute anisotropic diffusion coefficients that are in agreement with experimental data.

1. Introduction

Diffusion plays an important role in the kinetics of many materials processes. Experimental measurements of diffusion coefficients are expensive, difficult and in some cases nearly impossible. A complimentary approach is to determine diffusivities in materials by atomistic computer simulations. In addition to predicting diffusion coefficients, computer simulations can provide insights into atomic mechanisms of diffusion processes, creating a fundamental framework for materials design strategies.

Thanks to non equilibrium thermodynamics, the atomic transport theory is able to model the diffusion process in terms of atomic jump frequencies. In the linear response framework the diffusion coefficients, as was early shown [3,4], can entirely be expressed in terms of the commonly known Onsager coefficients L_{ij}. The L_{ij} are the fundamental kinetic quantities. In the context of the commonly known as multi-frequency model, originally developed by Le Claire [5], the Onsager coefficients for vacancy mediated diffusion can in turn be expressed in terms of frequency jumps rates of various atom-vacancy exchanges relative to a solute atom. For the case of isotropic alloys, the multi frequency models have been developed by Serruys and Brevec [6] for b.c.c. and by Allnatt [7,8] for f.c.c.

From the theoretical and modeling points of view, ab-initio methods are fundamental tools. Based on quantum mechanics, they calculate relevant magnitudes with a high degree of confidence. This allows not only to obtain specific numerical values but

* Corresponding author. Centro Atómico Constituyentes, Gerencia Física, Laboratorios Tandar, Av. General Paz 1499, C.P. 1650, San Martín, Argentina.
E-mail addresses: vpram@cnea.gov.ar (V.P. Ramunni), rivas@tandar.cnea.gov.ar (A.M.F. Rivas).

http://dx.doi.org/10.1016/j.matchemphys.2017.05.022
0254-0584/

also to gain in the understanding of the atomic level involved mechanisms. Furthermore, the molecular static technique known as the Monomer method [9] was developed to study the migration of defects in crystal systems. Knowing the energies and configurations of activated states, it is possible to study the atomic diffusion. Moreover, all these methods take advantage of parallel computer architectures (as clusters of PCs).

Recently, attempts were made in order to describe the diffusion process, in isotropic structures, by obtaining numerically the needed jump frequencies. Ad-initio based DFT calculations of diffusion coefficients where performed for b.c.c. alloys such as *Ni-Cr* and *Ni-Fe* [10], and for α*Fe-Ni* and α*Fe-Cr* alloys [4] as well as for *Mg*, *Si* and *Cu* diluted in f.c.c. *Al* [11]. Also, in a recent work Huang et al. [12], for *Fe* based diluted alloys, have performed DFT based calculations for the tracer diffusion coefficient with a larger number of atoms (128 instead of 54 as in [4]) that are in better agreement with the experimental data. On the other hand, one of us has recently shown [3] that, tracer diffusion coefficients performed with classical Molecular Static (MS) based calculations in diluted *Ni-Al* and *Al-U* f.c.c. alloys are in good agreement with available experimental data for both systems. Also diffusion in both f.c.c. and b.c.c. $Fe-Cr$ have been recently studied with great accordance between calculations and experimental data with classical MS calculations [13].

Hexagonally close packed (h.c.p.) structures have tetragonal symmetry and hence exhibit anisotropic diffusion properties. In this case, there are two independent diffusion coefficients: (i) diffusion coefficient, D_x, along a or b-axis direction i.e. along axes in the basal plane (ii) diffusion coefficient, D_z, along c-axis. Hence, five jump frequencies such as in the case of f.c.c. and b.c.c. are insufficient for describing diffusion in anisotropic structures such as h.c.p. The different types of jumps needed in this case are: (i) when the solute atom and the vacancy are within a basal plane (ii) when the solute and vacancy are in different basal planes, respectively. Thus, two sets of five, and two of the self-diffusion are needed to describe impurity diffusion in h.c.p. system.

The first attempts to describe diffusion kinetics in the anisotropic h.c.p. structure were performed by Ghate [1] and Batra [14] who used a model containing a total of eight atom vacancy jump frequencies to describe the solute correlation factor. Only recently DFT calculations of diffusivities in h.c.p structures using Ghate's [1] eight frequency model have been performed in *Mg* based alloys in Refs. [15] and [16]. In this last work, systematic comparison with experimental diffusion data show that the DFT based calculated diffusion coefficient are not always in agreement with the experimental data.

On the other hand, on the theoretical point of view, very recently Allnatt, Belova and Murch [2] have obtained, for h.c.p structures, expressions for the set of Onsager phenomenological coefficients in terms of a set of 13-frequencies. The 13-frequency model is a full description of the vacancy diffusion mechanism in the anisotropic h.c.p. crystallographic structure. This model goes beyond Ghate's eight frequencies one, but as was pointed in Ref. [2] a comparison of both formulations is not straightforward. However, results with both models need to be compare in order to understand the diffusion process in h.c.p. structures, as well as, the limitations of both models.

While the model by Allnatt et al. [2], in its most complete version involves 13 frequencies, in its current stage of development, there are only closed expressions for the tight-binding (TB) limit where all vacancies and solute atoms are paired. In this case, the model involves only 8 frequencies, although different from those used in the Ghate's model. A further simplification of the tight-binding limit of the 13 frequency model is applicable when the lattice parameters are close to ideal $c/a = \sqrt{8/3} \simeq 1.63299$. In this case, axial or basal jump frequencies are consider equals, so that diffusion coefficients depends on just five frequencies as in the f.c.c. model.

In this work, we perform numerical calculations of the diffusion coefficients for h.c.p. $\alpha Zr-Nb$ diluted alloys using both the 8-frequency model developed by Ghate [1] and the 13 frequency model (in the TB limit) recently developed by Allnatt et al. [2]. In order to exhaustively compare the diffusion coefficients obtained, with both models, we have performed the numerical calculations within a classical molecular static (MS) approximation, as well as, with two kinds of ab-initio first principles approaches, namely DFT with LDA and GGA approximations. Calculations with the Allnatt et al. [2] model are here applied to a specific alloy for the first time in the literature.

The choice of the $\alpha Zr-Nb$ alloys is based on that the alloy $Zr-2.5\%Nb$ is used in the manufacture of pressure tubes of the CANDU type nuclear power plants. Once on service, the pressure tubes are subjected to temperature and radiation, which modifies alloy's mechanical properties (yield stress) micro-structure, solubility and the diffusion coefficient. In particular, hydrogen related damage is related to the diffusion process. Hence diffusion properties in $Zr-Nb$ alloys deserve to be studied in order to evaluate their service lifetimes.

We have summarized the theoretical tools needed to express the diffusion coefficients in terms of microscopic magnitudes such as, the jump frequencies, the free vacancy formation energy and the vacancy-solute binding energy. Then we start with non-equilibrium thermodynamics in order to relate the diffusion coefficients with the phenomenological Onsager *L*-coefficients. The microscopic kinetic theory, allows us to write the Onsager coefficients in term of the jump frequency rates [7,8], which are evaluated from the migration barriers and the phonon frequencies under the harmonic approximation. The lattice vibrations are treated within the conventional framework of Vineyard [17] that corresponds to the classical limit.

In the present work, we employ DFT and classical molecular statics technique, both of them coupled to the Monomer method [9]. This much less computationally expensive method allows us to compute at low cost a bunch of jump frequencies from which we can perform averages in order to obtain more accurate effective frequencies.

We found that, our results for the *Nb* solute diffusion with MS calculations are not reliable, implying in the need for the development of accurate pseudo potentials in order to deal with *Nb* in the alloy. On the other hand, our calculations with LDA and GGA show that, *Nb* solute diffusion is well described by both, the Ghate's 8-frequencies model [1], and the Allnatt et al. [2] model of 13-frequencies in the tight-binding limit. Moreover, we show that the results obtained with the 5-frequency limit are in agreement with experimental data. Therefore, we can say that this simple model that does not take into account either the dissociation of pairs or anisotropy in the jump frequencies is sufficient to describe the anisotropic diffusion process in this h.c.p. alloy.

The paper is organized as follows: In Section II we briefly introduce a summary of the macroscopic equations of atomic transport that are provided by non-equilibrium thermodynamics [18–20]. In this way analytical expressions of the intrinsic diffusion coefficients in binary alloys in terms of Onsager coefficients are presented. Section III, is devoted to evaluate diffusion coefficients for the particular case of h.c.p diluted alloys. For this, we describe the expressions for the correlation factors and diffusion coefficients in terms of the jumps frequencies in the context of the 8-frequency model [1]. Then, we briefly describe the Allnatt et al. [2] 13 frequency model in the tight binding approximation and the way it

can be used to obtain correlation factors and the diffusion coefficients. In Section IV we describe the calculation details of the numerical methods used in this work in order to obtain the lattice parameters and energy jumps for the here studied $Zr-Nb$ diluted alloy. Our numerical results are presented in section V where we use the theoretical procedure here summarized and we perform a comparison of the results obtained with MS and DFT calculations within both, the 8 frequencies and the 13 frequencies models in the tight-binding and in the 5-frequency approximations. The last section is devoted to discussion of the results and conclusions.

2. Theory summary: the flux equations

Isothermal atomic diffusion in binary $A-S$ alloys can be described through a linear expression between the fluxes $\vec{J}_k$ and the driving forces related by the Onsager coefficients L_{ij} as,

$$\vec{J}_k = \sum_i^M L_{ki}\vec{X}_i, \tag{1}$$

where M is the number of components in the system, $\vec{J}_k$ describes the flux vector density of component k, while $\vec{X}_k$ is the driving force acting on component k. The second range tensor L_{ij} is symmetric ($L_{ij}=L_{ji}$) and depends on pressure and temperature, but is independent of the driving forces $\vec{X}_k$. For each k component, the driving forces may be expressed, in absence of external force, in terms of the chemical potential μ_k, so that [18],

$$\vec{X}_k = -T\nabla\left(\frac{\mu_k}{T}\right). \tag{2}$$

In (2) T is the absolute temperature, and the chemical potential μ_k is the partial derivative of the Gibbs free energy with respect to the number of atoms of specie k that is,

$$\mu_k = \left(\frac{\partial G}{\partial N_k}\right)_{T,P,N_{j\neq k}} = \mu_k^{\circ}(T,P) + k_B T\ln(c_k\gamma_k), \tag{3}$$

where k_B stands for the Boltzmann constant, γ_k, is the activity coefficients, which is defined in terms of the activity $a_k=\gamma_k c_k$ and c_k, is the molar concentration of specie k.

For the particular case of a binary alloy with N available lattice sites per unit volume, containing molar concentrations c_A for host atoms A, c_S of solute atoms S (impurities), the fluxes in terms of the Onsager coefficients are expressed as,

$$\mathbf{J}_A = -\frac{k_B T}{N}\left(\frac{L_{AA}}{c_A}-\frac{L_{AS}}{c_S}\right)\left(1+\frac{\partial\ln\gamma_A}{\partial\ln c_A}\right)\nabla c_A, \tag{4}$$

$$\mathbf{J}_S = -\frac{k_B T}{N}\left(\frac{L_{SS}}{c_S}-\frac{L_{AS}}{c_A}\right)\left(1+\frac{\partial\ln\gamma_S}{\partial\ln c_S}\right)\nabla c_S, \tag{5}$$

with

$$\mathbf{J}_V = -\mathbf{J}_A - \mathbf{J}_S, \tag{6}$$

for the flux of vacancies. From the flux Eqs. (4) and (5), the intrinsic diffusion coefficients for solvent A and solute S, are respectively defined as

$$D_A = \frac{k_B T}{N}\left(\frac{L_{AA}}{c_A}-\frac{L_{AS}}{c_S}\right)\phi_A, \tag{7}$$

and

$$D_S = \frac{k_B T}{N}\left(\frac{L_{SS}}{c_S}-\frac{L_{SA}}{c_A}\right)\phi_S. \tag{8}$$

In Eqs. (7) and (8), the quantities ϕ_A, ϕ_S are known as the thermodynamical factors,

$$\phi_A = \left(1+\frac{\partial\ln\gamma_A}{\partial\ln c_A}\right), \quad \phi_S = \left(1+\frac{\partial\ln\gamma_S}{\partial\ln c_S}\right). \tag{9}$$

In the dilute limit, the thermodynamics factor $\phi_A=\phi_S=1$, which simplifies the expression of the tracer diffusion coefficients in terms of the phenomenological coefficients.

Also, when species i performs n_i jumps of length a in time t, the L_{ij} coefficients can be expressed in terms of the so called collective correlation factors f_{ij} through [21].

$$L_{ii} = f_{ii}\frac{a^2 c_i n_i}{6k_B T t}\ ;\ L_{ij} = f_{ij}^{(i)}\frac{a^2 c_i n_i}{6k_B T t}\quad (i=A,S). \tag{10}$$

That is,

$$f_{AA} = \frac{k_B T}{N c_A}L_{AA}\left(\frac{1}{D_A^0}\right)\ ;\ f_{SS} = \frac{k_B T}{N c_S}L_{SS}\left(\frac{1}{D_S^0}\right), \tag{11}$$

and for the mixed terms,

$$f_{AS}^{(A)} = \frac{k_B T}{N c_A}L_{AS}^{(A)}\left(\frac{1}{D_A^0}\right) \quad ; \quad f_{AS}^{(S)} = \frac{k_B T}{N c_S}L_{AS}^{(S)}\left(\frac{1}{D_S^0}\right), \tag{12}$$

where $D_i^0 = a^2\Gamma_i/6$ $(i=A,S)$ are the diffusion coefficients of atoms of specie i in a complete random walk performing $\Gamma_i=\frac{n_i}{t}$ jumps of length a per unit time.

Murch and Qin [20] have shown that the standard intrinsic diffusion coefficients can be expressed in terms of the tracer diffusion coefficients $D_A^{\star}, D_S^{\star}$ which are measurable quantities, and the collective correlation factor f_{ij} $(i,j=A,S)$ as:

$$D_A = D_A^0\left[f_{AA}-\frac{c_A}{c_S}f_{AS}^{(A)}\right]\phi_A = D_A^{\star}\left[\frac{f_{AA}}{f_A}-\left(\frac{c_A}{c_S}\right)\frac{f_{AS}^{(A)}}{f_A}\right]\phi_A, \tag{13}$$

$$D_S = D_S^0\left[f_{SS}-\frac{c_S}{c_A}f_{AS}^{(S)}\right]\phi_S = D_S^{\star}\left[\frac{f_{SS}}{f_S}-\left(\frac{c_S}{c_A}\right)\frac{f_{AS}^{(S)}}{f_S}\right]\phi_S. \tag{14}$$

The intrinsic diffusion coefficients in (13) and (14) are known as the modified Darken equations. Also, for isotropic crystals, they express the tracer diffusion coefficients in terms of the tracer correlation factors f_A, f_S that are defined through [22].

$$D_i^{\star} = f_i D_i^0 = \frac{1}{6}\Gamma_i a^2 f_i, \quad (i=A,S). \tag{15}$$

To treat more general cases [22], in particular for anisotropic crystals, diffusion in any arbitrary direction can always be described in terms of diffusion coefficients only along the three principal axis. Several types of jumps may contribute to the diffusion in a given x-direction. A configuration of type α can perform jumps whose x component is x_α. Let Γ_α be its number of jumps in unit time. The tracer diffusion coefficients is expressed as a sum involving each jump type

$$D_x^* = \frac{1}{2}\sum_\alpha \Gamma_\alpha x_\alpha^2 f_x^\alpha, \tag{16}$$

where f_x^α are the partial correlation factors for each types of jumps.

Note the factor $\frac{1}{6}$ in (15), instead of $\frac{1}{2}$, that comes from the three dimensions involved in (15). Also, we can write a total correlation factor f_x such that

$$D_x^* = \frac{1}{2}\left(\sum_\alpha \Gamma_\alpha x_\alpha^2\right) f_x. \tag{17}$$

In this way, the total correlation factor f_x may be written in terms of the partial correlation factors f_x^α as

$$f_x = \frac{\sum_\alpha \Gamma_\alpha x_\alpha^2 f_x^\alpha}{\sum_\alpha \Gamma_\alpha x_\alpha^2}.$$

The number of jumps α in unit time is

$$\Gamma_\alpha = Z_\alpha C_\alpha \omega_\alpha \tag{18}$$

where C_α is the fraction of all configurations of type α, Z_α is the number of different (near neighbor sites) ways a jump of type α can occur and ω_α is the frequency for individual jump to occur in configuration of type α. The concentration of configurations of type α is [22].

$$C_\alpha = \exp\left(-\frac{\Delta G_\alpha^f}{k_B T}\right) = \exp\left(-\frac{\Delta H_\alpha^f - T\Delta S_\alpha^f}{k_B T}\right),$$

where ΔG_α^f is the Gibbs free energy for the formation of a type α configuration, while ΔH_α^f and ΔS_α^f stand for the formation enthalpy and entropy respectively. For vacancy mediated diffusion, C_α is the vacancy concentration near a jumping atom, hence

$$C_\alpha = C_V^{eq} \exp\left(-\frac{E_\alpha^b}{k_B T}\right),$$

where E_α^b is the binding energy between the pair formed by the vacancy and the jumping atom in the α configuration. The vacancy concentration at equilibrium is

$$C_V^{eq} = \exp\left(-\frac{E_V^f - TS_V^f}{k_B T}\right) \tag{19}$$

in terms of E_V^f and S_V^f the vacancy formation energy and entropy respectively. Hence, the α pair concentration is,

$$C_\alpha = \exp\left(-\frac{E_V^f - TS_V^f}{k_B T}\right)\exp\left(-\frac{E_\alpha^b}{k_B T}\right). \tag{20}$$

According to the transition-state theory, in a system of N atoms, the exchange frequency between a vacancy and an atom is,

$$\omega_\alpha = \nu_0 \exp\left(-\frac{G_\alpha^m}{k_B T}\right) = \nu_0 \exp\left(\frac{TS_\alpha^m - H_\alpha^m}{k_B T}\right). \tag{21}$$

In (21), G_α^m is the migration Gibbs free energy and the pre-exponential term, the "attempt frequency" ν_0, is of the order of the Debye frequency. The Gibbs free energy is given by $G_\alpha^m = H_\alpha^m - TS_\alpha^m$, where S_α^m is the migration entropy, while H_α^m is the enthalpy. As the volume is kept constant, $H_\alpha^m = E_\alpha^m$, where E_α^m is the internal migration energy. Hence, following Vineyard's formulation [17], the migration frequency jumps are given by

$$\omega_\alpha = \nu_0^\star \exp(-E_\alpha^m/k_B T). \tag{22}$$

In (22), E_α^m are the vacancy migration energies at $T = 0K$, while

$$\nu_\alpha^\star = \left(\prod_{i=1}^{3N-3} \nu_i^I\right)_\alpha \Big/ \left(\prod_{i=1}^{3N-4} \nu_i^S\right)_\alpha = \nu_0 \exp\left(\frac{S_\alpha^m}{k_B}\right), \tag{23}$$

with ν_i^I and ν_i^S the frequencies of the normal vibrational modes at the initial and saddle points, respectively.

3. The impurity diffusion coefficients in h.c.p. lattices $D_\parallel$ and $D_\perp$

For the case of hexagonal closed packed (h.c.p.) structures, such as *Zr*, the crystal anisotropy results in two independent diffusion coefficients. Diffusion parallel to the c axis, (1D diffusion along z−axis) called $D_\parallel$, that occurs only by inter-basal (or axial) jumps, while diffusion perpendicular to the c axis (2D diffusion in the xy−plane) called $D_\perp$, can occur either by basal jumps, or by a series of inter-basal jumps (see Fig. 2). Basal jumps generate atomic displacements of magnitude a on the basal plane, whereas inter-basal jumps generate atomic displacements in $c/2$ parallel to the axial direction, along with displacements in $a/\sqrt{3}$ perpendicular to such direction, where a and c are the h.c.p. lattice parameters. Hence, for the axial diffusion,

$$D_\parallel^* = \frac{1}{2} f^z \sum_\alpha^{axial} \Gamma_\alpha \frac{c^2}{4} \tag{24}$$

where the sum in (24) runs on the axial jumps. For on plane diffusion

$$D_\perp^* = \frac{1}{4}\left(f_b^x \sum_\alpha^{basal} \Gamma_\alpha a^2 + f_a^x \sum_\alpha^{axial} \Gamma_\alpha \frac{a^2}{3}\right) \tag{25}$$

where the first summation in (25) runs on the basal jumps and the second on axial ones.

In this work, we perform a comparison between two formalism in order to calculate the diffusion coefficients in h.c.p. structures. In first place, the Ghate's 8-frequency model, gives expressions for the partial correlation factors f_a^x, f_b^x, and f^z. While in 13-frequency model developed by Allnatt, Belova and Murch [2], the diffusion equations are expressed in terms of total correlation factors f^z and f^x, that is,

$$D_\parallel^* = \frac{1}{2} f^z \sum_\alpha^{axial} \Gamma_\alpha \frac{c^2}{4} \tag{26}$$

where now the sum in (26) runs on the axial jumps involving the 13-frequencies. While the plane diffusion

$$D_\perp^* = \frac{1}{4} f^x \left(\sum_\alpha^{basal} \Gamma_\alpha a^2 + \sum_\alpha^{axial} \Gamma_\alpha \frac{a^2}{3}\right) \tag{27}$$

is expressed in terms of the total correlation factor f_z.

In diluted binary $A - S$ alloys, a very small concentration of vacancies, V, transports the atoms by nearest-neighbor (NN) exchanges. A vacancy, V, and a solute atom, S, interact only when they are nearest-neighbors, then a $V - S$ pair is formed. Such a pair is said to be bounded for attractive as well as for repulsion interaction between V and S. In h.c.p. structures, we distinguish between type a pairs, p_a, in which the S and V are in adjacent hexagonal (basal) planes and type b pairs, p_b, in which they are in the same basal plane. Similarly as for the 5-frequency f.c.c. model definitions of the atom-vacancy exchange frequencies jump rates are: ω_2 for a

vacancy-solute exchange, ω_1 a vacancy-host exchange which merely reorients a bound pair, ω_3 for a vacancy-host exchange which takes the vacancy from a bound to an unbound state, ω_4 for the inverse of a ω_3 jump and ω_0 for a vacancy-host exchange in which the vacancy passes between unbound sites. For the h.c.p. model, Allnatt et al. [2], have retained the same subscript meanings but a prime superscript is added for vacancy jumps between adjacent hexagonal planes (out-of-plane jumps), while no prime is added if the vacancy remains in the same hexagonal plane (in-plane jumps). Also, as in Ref. [2], a subscript *a* or *b* is added that indicates the type of pair concerned. Fig. 1, depicts the jump rates ω_i and ω_i' $(i = 1, 2, 3, 4)$ considering only jumps between first neighbors. There are also in-plane, ω_0, and out-of-plane, ω_0', jumps of the vacancy between unbound sites.

3.1. The 8-frequency model of Ghate

Single vacancy diffusion in pure structures: For self-diffusion, all vacancy jumps are equally probable, and so the correlation factor has a constant value that depends only on the geometry of the crystal lattice. Total jump frequency, $\Gamma = Z\omega$, where Z is the number of NN sites into which a vacancy can jump to and ω is the frequency for individual jumps. As we mentioned earlier, an h.c.p. lattice has 6 in-plane and 6 out-of-plane NN sites, $Z_a = Z_b = 6$. Also, the jumps between a vacancy V and a solvent atom can be, in-plane with individual frequency ω_0, or out-of-plane, with individual frequency ω_0'. Substituting for Γ in Eqs. (24) and (25) the self-diffusion coefficients for the pure structure are obtained as

$$D_{A\parallel}^{*} = \frac{3}{4} c^2 f_A^z C_V \omega_0' \,, \tag{28}$$

and

$$D_{A\perp}^{*} = \frac{1}{2} a^2 C_V \left(f_{Ab} \omega_0' + 3 f_A^x \omega_0 \right) . \tag{29}$$

In (28) and (29), ω_0 and ω_0' are respectively, the individual jump frequencies in the axial and basal planes of the pure h.c.p. matrix, calculated from (22) and (23). As in Ref. [23] the correlation factors f_A^z, f_A^x and f_{Ab} are presently set to the f.c.c. constant value $f = 0.78$. The vacancy concentration C_V is obtained from (19). The presence of a solute, however, can alter the vacancy motion by biasing certain jumps. If the solute-vacancy exchange frequency is much smaller (larger) than other vacancy exchanges, the values of f can be increased (decreased) relative to that of self-diffusion. The degree to which this effect hinders diffusion depends on the correlation of vacancy positions between two consecutive solute-vacancy exchanges.

For the solute diffusion, the solute correlation factors f_S^z, f_S^z and f_{Ab} are inserted in Eqs. (24) and (25) such that,

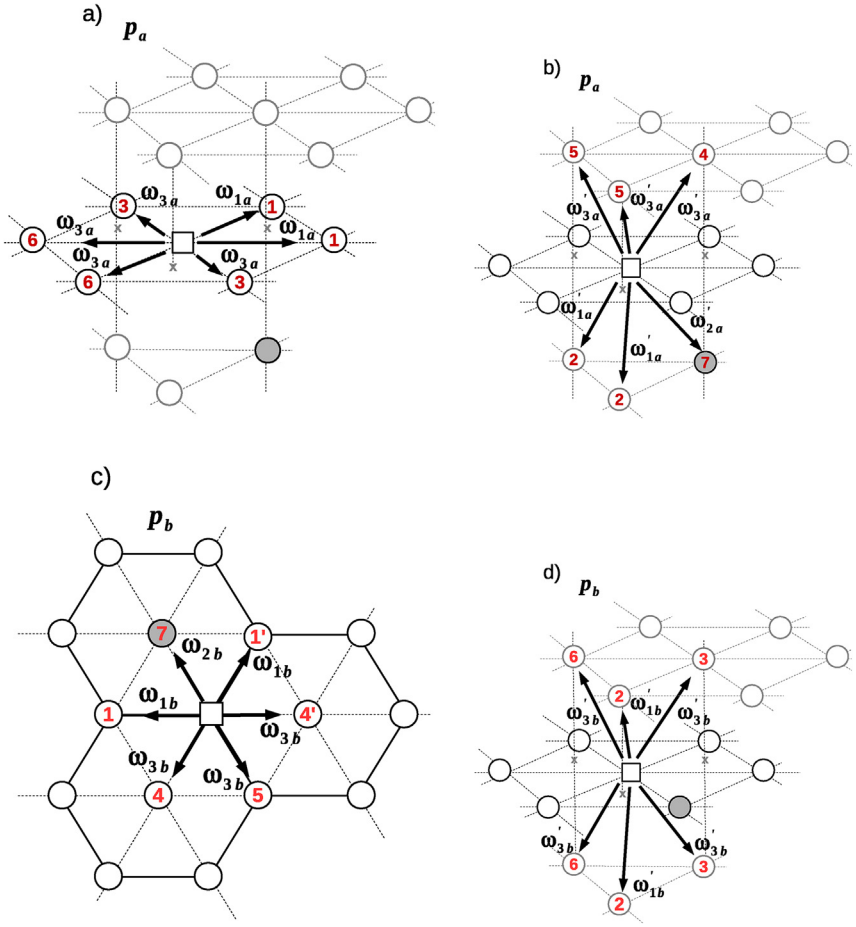

Fig. 1. a) In plane vacancy jumps in the thirteen-frequency model [2] from the p_a configuration $(2\omega_{1a}, 4\omega_{3a})$. b) Out of plane vacancy jumps in the thirteen-frequency model [2] from the p_a configuration $(\omega'_{2a}, 2\omega'_{1a}, 3\omega'_{3a})$. c) In plane vacancy jumps in the thirsteen-frequency model [2] from the p_b configuration $(\omega_{2b}, 2\omega_{1b}, 3\omega_{3b})$. d) Out of plane vacancy (only shown for $z > 0$) jumps in the thirsteen-frequency model [2] from the p_b configuration $(2\omega'_{1b}, 4\omega'_{3b})$.

$$D^{*}_{S\parallel} = \frac{3}{4}c^2 C_a f^z_S \omega'_{2a}, \tag{30}$$

$$D^{*}_{S\perp} = \frac{3}{2}a^2 C_b f^x_S \omega_{2b} + \frac{1}{2}a^2 C_a f_{Ab} \omega'_{2a}. \tag{31}$$

Again, a and c are the lattice parameters, ω_{2b} and ω'_{2a} are the solute-vacancy exchange jump frequencies within and out of the basal plane. The concentrations C_a and C_b for the axial an basal pairs are obtained from Eq. (20) with the corresponding axial and basal binding energies respectively. The solute correlation factors, f^i_S, f_{Ab} $(i = x, z)$, in (30) and (31), can be quantitatively evaluated using a multi-frequency models well known as the 8-frequency model developed for the h.c.p. lattice by Ghate [1], which is analogous to the 5-frequency model of Le Claire for f.c.c. metals [5]. In this case, the model is based on 8 of the above described frequencies, which are $(\omega'_{2a}, \omega'_{1a}, \omega_{1a}, \omega_{3a})$ and $(\omega_{2b}, \omega'_{1b}, \omega_{1b}, \omega_{3b})$. The solute correlation factors that depend on the 8 jump frequencies illustrated in Fig. 1 are given by (see [1])

$$f^z_S = \frac{2\omega'_{1a} + 5.152\omega_{3a}}{2\omega'_{1a} + 5.152\omega_{3a} + 2\omega'_{2a}}, \tag{32}$$

$$f^x_S = 1 + \frac{2S_{Sx}}{\lambda_B}, \tag{33}$$

$$f_{Ab} = 1 + \frac{2S_{Ab}}{\lambda_{Ab}}. \tag{34}$$

The distances, $\lambda_B = a$ for a jump within the basal plane and $\lambda_{Ab} = a/\sqrt{3}$, the projection of the axial jump onto a basal plane are depicted in Fig. 2, and the lengths S_{Bx} and S_{Ab} are determined by

$$S_{Sy} = \frac{\omega'_{1b}S_{Ab} - \omega_{1b}S_{Sy}}{2\omega'_{1b} + 2\omega_{1b} + 5.152\omega_{3b} + \omega_{2b}}, \tag{35}$$

$$S_{Sx} = \frac{\sqrt{3}\omega'_{1b}S_{Ab} + \omega_{1b}S_{Sx} - \omega_{2b}(\lambda_B + S_{Sx})}{2\omega'_{1b} + 2\omega_{1b} + 5.152\omega_{3b} + \omega_{2b}}, \tag{36}$$

$$S_{Ab} = \frac{\omega'_{1a}\left(\sqrt{3}\,S_{Sx} + S_{Sy}\right) - \omega_{1a}S_{Ab} - \omega'_{2a}(\lambda_{Ab} + S_{Ab})}{2\omega'_{1a} + 2\omega_{1a} + 5.152\omega_{3a} + \omega'_{2a}}, \tag{37}$$

After solving this system of linear equations simultaneously, one can substitute the results into Eqs. (32–34) in order to obtain the correlation factors that are functions only of the various ratios of jump frequencies and the ratio λ_B/λ_{Ab}.

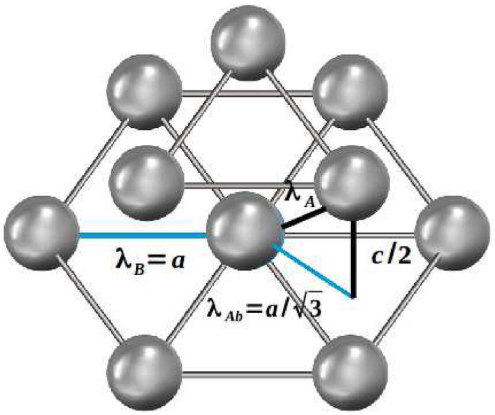

Fig. 2. h.c.p. jump distances used in the 8-frequency model [15].

3.2. The 13-frequency model of Allnatt

Recently, a more complete model, involving 13 frequencies, has been developed by Allnatt, Belova and Murch [2] for the diffusion process for h.c.p. lattices. Then, the effect of different vacancy exchange mechanisms on diffusion, can be described with an effective 13 frequency model [2]. As we have already mentioned, similarly as for the 5-frequency f.c.c. model definitions of the atom-vacancy exchange frequencies jump rates are: ω_2 for a vacancy-solute exchange, ω_1 a vacancy-host exchange which merely reorients a bound pair, ω_3 for a vacancy-host exchange which takes the vacancy from a bound to an unbound state, ω_4 for the inverse of a ω_3 jump and ω_0 for a vacancy-host exchange in which the vacancy passes between unbound sites. For the h.c.p. model, Allnatt et al. [2], have retained the same subscript meanings but add a superscript prime if the vacancy jumps between adjacent hexagonal planes (out-of-plane jumps), but not if the vacancy remains in the same hexagonal plane (in-plane jumps). They have also added a subscript a or b in order to indicate the type of pair concerned. Fig. 1, depicts the jump rates ω_i and ω'_i $(i = 1, 2, 3, 4)$ considering only jumps between first neighbors.

For p_a type of pairs, there are six possible in-plane vacancy jumps $(2\omega_{1a}, 4\omega_{3a})$ and six possible out-of-plane jumps $(\omega'_{2a}, 2\omega'_{1a}, 3\omega'_{3a})$. Analogously, for pairs of type p_b, there are six possible in-plane vacancy jumps $(\omega_{2b}, 2\omega_{1b}, 3\omega_{3b})$ and six possible out-of-plane jumps $(2\omega'_{1b}, 4\omega'_{3b})$. The full set of frequencies are depicted in Fig. 1. Corresponding to the four kinds of dissociation jump (the four exchange frequencies each with a subscript 3), there are four kinds of association jump which are jumps in the reverse sense of jumps 3 with a subscript 4. There are also in-plane, ω_0, and out-of-plane, ω'_0, jumps of the vacancy between unbound sites. The principle of detailed balance shows that among the 16 jump frequencies just defined, there are three independent relations:

$$\frac{\omega_{4X}}{\omega_{3X}} = \frac{\omega'_{4X}}{\omega'_{3X}} = \exp\left(-\beta E^b_X\right), \quad X = a, b \tag{38}$$

$$\frac{\omega'_{1a}}{\omega'_{1b}} = \frac{\exp\left(-\beta E^b_b\right)}{\exp\left(-\beta E^b_a\right)} = \frac{\omega'_{4b}/\omega'_{3b}}{\omega'_{4a}/\omega'_{3a}} \tag{39}$$

This leaves 13 independent frequencies.

3.2.1. Isotope-limit case: the tracer self-diffusion

Self diffusion can be studied in the isotope-limit, defined as the case where the solute, S, is an isotope of the solvent, A, so that all exchange frequencies are either ω_0 or ω'_0, according to them being in-plane or out-of-plane jumps. In this case, the correlation factor, f^x and f^z, varies with the frequency ratio $x = \omega_0/\omega'_0$ such that correlation factor for the pure Zr in the z and x components are respectively

$$f^z = \left(1 + 8.77x + 7.37x^2 + 0.65x^3\right)\Big/\left(1 + 9.90x + 10.90x^2 + x^3\right), \tag{40}$$

$$f^x = \left(0.56 + 4.38x + 3.67x^2 + 0.64x^3\right) \Big/ \left(1 + 5.75x + 4.11x^2 + x^3\right). \tag{41}$$

$$\frac{L_{SS}^{(0)z}}{L_{AA}^{(0)z}} = \frac{\omega'_{2a}}{4\omega'_{1a}} \tag{47}$$

Similarly, for the x-direction:

$$f_S^x = \frac{3\left[H\omega_{1a}\left(F\omega_{1b} + 2\omega'_{1b}(F + \omega'_{2a}\omega_{2b})\right) + 2G_{1b}\omega'_{1a}\left(\omega'_{1b}\omega'_{2a}\omega_{2b} + \omega_{1b}(F + 3\omega'_{2a}\omega_{2b})\right)\right]}{F\left[3G_{12b}H\omega_{1a} + 2\left(G_{12b}H\omega'_{2a} + 3\omega'_{1a}\left(\omega'_{1b}\omega_{2b} + \omega_{1b}(G_{1b} + 2\omega_{2b})\right)\right)\right]} \tag{48}$$

In this limit, the matrix method gives that the cross collective correlation factor $f_{AS}^{(S)i} = (1 - f_i)$, with $i = x, z$. In the isotopic limit the tracer self-correlation factors f^z, f^x are calculated from (40) and (41). This expressions of the correlation factors are then inserted in expressions (26) and (27) in order to obtain the tracer self-diffusion coefficients

$$D_{\parallel}^* = \frac{3}{4}c^2 f^z C_V \omega'_0, \tag{42}$$

in the axial direction and

$$D_{\perp}^* = \frac{1}{2}a^2 f^x C_V(\omega'_0 + 3\omega_0), \tag{43}$$

for the plane diffusion.

3.2.2. The tight-binding approximation: self- and impurity diffusion coefficients

As we have already mentioned, in the current stage of development of the 13-frequency model, Allnatt et al. have obtained closed expressions for the correlation factors only in the tight-binding (TB) limit where all vacancies and solute atoms are paired. In this case, both $-E_a^b$ and $-E_a^b$ are so large that all the vacancies are always bound to the solute atoms (Tight-binding case), it is also assumed that the concentration of vacancies is never greater than the concentration of the solute atoms. Under this assumption, the effect of sources and sinks can only be reflected in the total vacancy concentration.

In this limit, the solvent and solute fluxes $\mathbf{J}_A$, and $\mathbf{J}_S$ are not independent. The vacancy mechanism ensures $\mathbf{J}_A + \mathbf{J}_S + \mathbf{J}_V = 0$, and the tight binding condition implies in $\mathbf{J}_S = \mathbf{J}_V$. It is then shown in Ref. [2] that in the tight-binding limit, two collective correlation functions are simply related to the solute correlation factor:

$$f_{AS}^{(S)i} = -2f_S^i, \tag{44}$$

$$f_{AA}^i = 4\left(L_{SS}^{(0)i} \Big/ L_{AA}^{(0)i}\right) f_S^i, \quad i = x, z \tag{45}$$

with $L^{(0)}$ corresponds to the, so called, uncorrelated part of L-coefficients. For migration in the z-direction, the solute correlation factor has been obtained in Ref. [2], to be:

$$f_S^z = \frac{\omega'_{1a}}{\omega'_{1a} + \omega'_{2a}} \tag{46}$$

and, the required ratio of the uncorrelated parts is:

with

$$H = 3\omega_{1b} + 2\omega'_{1b}\,; \tag{49}$$

$$F = \omega'_{1b}\omega'_{2a} + 3\omega'_{1a}\omega_{2b}\,; \tag{50}$$

$$G_{1b} = \omega_{1b} + \omega'_{1b}\,; \tag{51}$$

$$G_{12b} = \omega_{1b} + 2\omega'_{1b} + 2\omega_{2b}\,. \tag{52}$$

and

$$\frac{L_{SS}^{(0)x}}{L_{AA}^{(0)x}} = \frac{\left(3\omega'_{1a}\omega_{2b} + \omega'_{2a}\omega'_{1b}\right)}{2\left[\omega'_{1a}\left(3\omega_{1b} + \omega'_{1b}\right) + \omega'_{1b}(3\omega_{1a} + \omega'_{1a})\right]}\,. \tag{53}$$

The solute correlation factors f_S^i , for $i = z, x$, are obtained with the help of Eqs. (46) and (48) respectively. This expressions of the solute correlation factors are then inserted in expressions (26) and (27) in order to obtain the solute diffusion coefficient in the z direction

$$D_{S\parallel}^* = \frac{3}{4}c^2 f_S^z C_a \omega'_{2a}, \tag{54}$$

and for the plane diffusion

$$D_{S\perp}^* = \frac{1}{2}f_S^x a^2(3C_b\omega_{2b} + C_a\omega'_{2a}). \tag{55}$$

The pair concentrations C_a and C_b for the axial and basal pairs p_a, p_b (see Fig. 1) are obtained from Eq. (20) with the corresponding axial and basal binding energies respectively.

Also, using relation (45) with the solute correlation factors f_S^i from (46) and (48) together with the expressions (47) and (53), we obtain the solvent correlation factors f_A^i for $i = z, x$, respectively. In this way, the solvent diffusion coefficients in the alloy are obtained as

$$D_{A\parallel}^{\bigstar} = \frac{3}{4}c^2 f_A^z C_a \omega'_0, \tag{56}$$

$$D_{A\perp}^{\bigstar} = \frac{1}{2}a^2 f_A^x(C_a\omega'_0 + C_b 3\omega_0). \tag{57}$$

Note that, in the tight-binding limit here described, only eight frequencies are involved in order to obtain the diffusion coefficients, they are ω_{1a}, ω'_{1a}, ω_{1b}, ω'_{1b}, ω'_{2a}, ω_{2a}, as well as, ω_0 and ω'_0. Differently from the 8-frequency model by Ghate [1] the frequencies ω_{3a} and ω_{3b} are not involved, as they correspond to

dissociative jumps.

For an ideal h.c.p. structure ($c/a = \sqrt{8/3} \simeq 1.63299$) the two nearest-neighbor jump distances are then equal. For this case, we can put the two migration energies equal to obtain just 5-frequencies as in the f.c.c. model. (i.e. put ω_{1a}, ω'_{1a}, ω_{1b}, and ω'_{1b} all equal to ω_1 while ω'_{2a} and ω_{2b} are set equal to ω_2). This is called the 5-frequency model. Exploring the 5-frequency model of the tight-binding approximation, the results for z-axis migration are, as usual, the same as those for the 5-frequency f.c.c. model that is:

$$f_S^{5f,z} = \frac{\omega_1}{\omega_1 + \omega_2} \tag{58}$$

and

$$f_{AA}^{5f,z} = \frac{\omega_2}{\omega_1 + \omega_2}, \tag{59}$$

as in (44), $f_{AS}^{5f,z} = -2f_S^{5f,z}$. But for the x-axis the solute correlation factors differ, that for the h.c.p. case being:

$$f_S^{5f,x} = \frac{3\omega_1(38\omega_1 + 13\omega_2)}{2(57\omega_1^2 + 78\omega_1\omega_2 + 20\omega_2^2)}, \tag{60}$$

also, $f_{AS}^{5f,x} = -2f_S^{5f,x}$. Expression for the 5-frequency limit for the x-axis $f_{AA}^{5f,x}$ is:

$$f_{AA}^{5f,x} = \frac{3\omega_2(38\omega_1 + 13\omega_2)}{2(57\omega_1^2 + 78\omega_1\omega_2 + 20\omega_2^2)}. \tag{61}$$

It is important to note that, in the 5-frequency model for the tight-binding approximation here described, the diffusivities only depend on 3 frequencies, which are (ω_0, ω_1, and ω_2).

In order to study the diffusion process in h.c.p diluted alloys, in the next section we perform numerical calculations that provide the different quantities needed to express the diffusion coefficients. The numerical calculations provide, the vacancy formation energy and entropy, from which the vacancy concentration C_V is obtained through (19), the binding energy between $V - S$ pairs, from which pair concentrations C_a and C_b are obtained from Eq. (20). While the individual jump frequencies are calculated from (22) and (23) once the vacancy migration energies and entropies are numerically obtained. In the following sections we obtain, for $Zr - Nb$ diluted alloys, the correlation factors and diffusion coefficients described in the present section.

4. Calculation methods

Most of the DFT results in *Zr* reported here have been obtained with the SIESTA code based on numerical, localized, atomic orbitals and pseudopotentials [24]. The current calculations have been performed within the generalized gradient approximation (GGA) and the local density approximation (LDA) for exchange and correlation with the inclusion of semicore states ($4s^2 4p^6$ for Zr). The orbital basis used can be described as DZ with a polarized 5*s* state for Zr. For Nb we use the pseudopotentials and basis sets from the SIESTA home page. This method is very efficient at obtaining the equilibrium positions of the atoms by relaxing the structure via the conjugate gradients technique. The force convergence is chosen as 0.02 eV/Å. A spatial mesh cutoff of 450.0 Ry is used, with a smearing temperature of 0.15 eV, within a Fermi-Dirac scheme. Reciprocal space is partitioned in a $4 \times 4 \times 4$ Monkhorst-Pack grid. The current super-cell of 48 *Zr* atoms, eventually including one *Nb* atom, represents a concentration of 2 at.% of Nb. Though apparently the *Nb* atoms are already far enough in the periodical repetitions to make their interaction negligible.

Complementary, DFT calculations with VASP, were used to corroborate some structure energies in the projector augmented wave (PAW) framework with a kinetic-energy cutoff of 460 eV in the generalized gradient approximation (GGA) using PAW-PBE functionals. The current super-cell of 144 *Zr* atoms, as with SIESTA, eventually including one Nb atom. The Brillouin zone was sampled with a $2 \times 2 \times 2$ mesh k-points. The plane-wave cutoff energy in the expansion of the wave functions was set to 460 eV. Geometry optimizations were converged so that the largest forces did not exceed 0.02 eV/Å. Note that, the energies can be modified by changing the number of atoms used in the simulation [3]. Therefore, in order to verify the stability of the our results, calculations with VASP employ a greater number of atoms.

In addition, classical calculations were also performed using EAM potentials, developed by Pasianot and Monti [27,28], for the pure elements *Zr* and *Nb*, as well as, for the cross $Zr - Nb$ term. The EAM interatomic potential, reproduces room temperature elastic behavior for α-Zr. The simulation crystallite was formed by $7 \times 4 \times 4$ unit cell containing 448 atoms. Impurity and defect relaxation, as before, includes one substitutional *Nb* atom in *Zr*, as well as, a single vacancy.

Several efficient methods have been developed in recent years for finding activated states or, mathematically, saddle points [29]; here we employ the Monomer coupled to SIESTA and MS techniques, developed previously in our laboratory [23]. Its coupling to an ab initio code using SIESTA's facility to be interfaced as a subroutine (SIESTA as a subroutine feature). The Monomer computes the least local curvature of the potential energy surface using only the forces furnished by SIESTA.

The Monomer Method [9], is a static technique to search the potential energy surface for saddle configurations, thus providing detailed information on transition events. The Monomer computes the least local curvature of the potential energy surface using only forces. The force component along the corresponding eigenvector is then reversed (pointing “up hill”), thus defining a pseudo force that drives the system towards saddles. Both, local curvature and configuration displacement stages are performed within independent conjugate gradients loops. The method is akin to the Dimer one from the literature [29], but roughly employs half the number of force evaluations which is a great advantage in ab-initio calculations.

Finally, our calculations are carried out at constant volume, and therefore the enthalpic barrier $\Delta H = \Delta U + p\Delta V$ is equal to the internal energy barrier ΔU.

5. Results

As we have already mentioned, in a recent work Allnat et al. [2] show that to fully consider the anisotropy of an h.c.p. lattice, 13 independent atom-vacancy exchange frequencies are needed in contrast to the 8-frequency model developed by Ghate [1]. Here we explore both models to study diffusion driven by vacancies in h.c.p. $Zr - Nb$ diluted alloy. In this section we display the results of our numerical calculations for both multi-frequency models and performed with classical MS, and with two quantum DFT approximations, namely LDA and GGA.

In Table 1 we display the results obtained for the h.c.p lattice parameter a and for the ratio c/a that minimizes the crystal structure energy together with their respective experimental values.

Table 1 shows that results from DFT calculations with LDA, give an ideal ratio $c/a = 1.63$, while MS gives a more realistic $c/a = 1.59$

Table 1
Lattice parameters of αZr in Å from MS and DFT calculations. Experimental values exactly fitted in Ref. [27]. E_c the cohesive energy.

	a (Å)	c/a	$E_c(eV)$
Exp.	3.232	1.59	6.25
MS	3.232	1.59	6.25
DFT (LDA)	3.130	1.63	
DFT (GGA)	3.217	1.62	

ratio for αZr. The GGA approximation gives an intermediate value of $c/a = 1.62$.

Dependencies of the lattice parameter a and structural relation c/a for the h.c.p. $Zr-Nb$ alloys versus Nb concentration were calculated by Kharchenco and Kharchenco [30], using DFT calculations at zero temperature. The here performed calculations for a and ratio c/a in αZr, are in agreement with results in Ref. [30].

Once the h.c.p. lattice has been constructed, in Table 2 we summarizes the computed magnitudes for vacancy formation and migration energies $E(eV)$ and entropies S (Boltzmann's constant, k_B), together with the attempt mean jump frequency, $\nu^\star = \nu_0 \exp(S_m^V/k_B)$, for pure αZr. Present calculations also include some configuration energies verified using VASP.

For MS, the vacancy formation energy (E_f^V) in Table 2 for pure Zr is calculated as $E_f^V = E(N-1) + E_c - E(N)$, where $E(N)$ is the energy of a perfect lattice with N atoms, $E(N-1)$ is the energy of the defective system, and E_c the cohesion energy. The vacancy migration barrier in perfect lattice, E_m^V, is calculated with the Monomer method [9], and the activation energy, E_Q, is then obtained as, $E_Q = E_f^V + E_m^V$. While, for DFT calculations E_f^V is calculated as,

$$E_f^V = E(N-1) - (N-1)*E(N)/N. \quad (62)$$

Our calculations of the vacancy formation and migration energies in pure Zr are shown in Table 2, together with previous calculations. With classical MS we obtain a formation energy of $2.01eV$. The SIESTA code, within the LDA and GGA approximation, gives respectively formation energies of $1.98eV$ and $2.1eV$. This last value is quite in accordance with the formation energy of $2.06eV$ obtained in the GGA approximation with VASP code. Note also, the stability of the results with the change of the number of atoms.

The migration jump is anisotropic, as was shown previously in Ref. [26]. In our calculations it requires 0.59, 0.55 or $0.50eV$ for the basal direction, and 0.61, 0.62 or $0.53eV$ for the axial one, respectively for MS and DFT with LDA or GGA calculations.

Therefore, the activation energies for Zr self-diffusion, for the basal/axial direction, predicted by MS are $2.61/2.63(eV)$, and $2.53/2.60(eV)$ or $2.60/2.63(eV)$ respectively for LDA or GGA approximations. Previous results of the barriers with WIEN2k within the LDA approximation, results in $2.37/2.43eV$ [23].

Energies in Table 2 are modified by the presence of impurities. For the case of diluted alloys, we consider the presence of solute vacancy complexes, $C_n = S + V_n$, in which $n = 1^{st}, 2^{nd}, 3^{rd}, \ldots$ indicates that the vacancy is a $n-$ nearest neighbors of the solute atom S. Here, impurity diffusion in αZr is characterized by substitutional diffusion atoms of Nb, driven by vacancies. The binding energy, E_α^b, between the solute and the vacancy for the complex $C_n = S + V_n$ in a matrix of N atomic sites is obtained as,

$$E_\alpha^b = \{E(N-2, C_n) + E(N)\} - \{E(N-1, V) + E(N-1, S)\}, \quad (63)$$

where $E(N-1,V)$ and $E(N-1,S)$ are the energies of a crystallite containing $(N-1)$ atoms of solvent A plus one vacancy V, and one solute atom S respectively, while $E(N-2, C_n)$ is the energy of the crystallite containing $(N-2)$ atoms of A plus one solute vacancy complex $C_n = S + V_n$. With the sign convention used here $E_b < 0$ means attractive solute-vacancy interaction, and $E_b > 0$ indicates repulsion. Table 3 displays for $Zr-Nb$, the binding energies E_α^b of the different type of solute vacancy pairs p_a or p_b.

The calculated vacancy-solute binding energies, E_b, summarized in Table 3 show that, with MS calculations, we have obtained a strong repulsive interaction between vacancy and Nb atoms $E_b > 0$. While quantum results (with both LDA and GGA) give $E_b < 0$. For both LDA and GGA approximations E_b reveal a weak attractive interaction between vacancy and solute in the case of $Zr-Nb$. Also, the binding energies, for the GGA approximation, obtained with SIESTA and with VASP codes are in good accordance.

In Ref. [36], the properties of simple point defect (i.e. vacancy, self and foreign interstitial atoms) in the h.c.p. (α) and b.c.c. (β) Zr with trace solute Nb have been studied by ab initio calculations with VASP codes. The calculations indicate that the formation energies of vacancy and substitutional Nb atom are $1.94eV$ and $0.68eV$ in αZr and $0.36eV$ and $0.07eV$ in βZr, respectively, while the binding energies of the nearest neighbor vacancy-substitutional Nb pair and the nearest neighbor substitutional $Nb-Nb$ pair are $0.09eV$ and $0.03eV$ in alpha αZr and $2.78eV$ and $0.72eV$ in βZr, respectively.

These results suggest that the Nb atoms are more likely to agglomerate and form precipitates in βZr than in αZr. Thus, the α-Zr-β-Zr-β-Nb transition mechanism through in situ α to β transformation of Zr and the vacancy-assisted Nb diffusion for Nb conglomeration in βZr under irradiation is proposed to explain the existence of βNb and Zr precipitate mixtures observed in the

Table 2
Computed magnitudes for vacancy formation and migration: energies E (eV) and entropies S (Boltzmann's constant, k_B) in pure Zr with SIESTA + Monomer. The attempt mean jump frequency ($\nu^\star = \nu_0 \exp(S_m^V/k_B)$). Columns labeled Vac, A-jump and B-jump refer to the relaxed vacancy, non-basal (ω_0') and basal (ω_0) jumps, respectively. Previous results in column five.

MS	Vac	A-jump	B-jump	Refs.
$E(eV)$	1.74	0.59	0.57	[27]
	2.02	0.61	0.59	[28]
	2.01	0.61	0.59	Current
$S(k_B)$	1.15	6.36	5.93	Current [27],[27]
$\nu^\star(THz)$		19.2	16.1	[33]
DFT	Vac	A-jump	B-jump	Refs.
$E(eV)$	2.34	0.51	0.37	[23]
	1.90	0.57	0.39	[31]
	1.98	0.62	0.55	Current LDA
	2.1	0.53	0.50	Current GGA
	2.06			Current GGA (VASP)
$S(k_B)$(LDA)	1.51			Current LDA
$S(k_B)$(GGA)	2.0			Current GGA
$\nu^\star(THz)$(GGA)		18.56	14.77	[34]
MD	Vac	A-jump	B-jump	Refs.
$E(eV)$		0.53	0.51	[33]
$E(eV)$ Exp.	>1.58			[35]

Table 3
Binding energies, E_α^b (in eV), for p_a and p_b^j ($j = 1, 1'$).

	n	MS	LDA	GGA	GGA
				SIESTA	VASP
p_a	1	0.245	−0.051	−0.073	−0.067
p_b	1	0.228	−0.044	−0.091	−0.094
	1′	0.423	−0.071	−0.093	

Table 4
Migration energies E_m (in eV) for vacancy jumps in $Zr-Nb$ from classical and quantum calculations coupled to the Monomer. In bold the barriers involved in the 8-frequency model by Ghate [1].

$Zr-Nb$				
n	ω_j	**MS**	**LDA**	**GGA**
	ω_0	0.59	0.55	0.50
	ω'_0	0.61	0.62	0.54
1	$\omega_{\mathbf{1a}}$	0.50	0.20	0.21
2	$\omega'_{\mathbf{1a}}$	0.30	0.26	0.32
3	ω^3_{3a}	0.68	0.48	0.66
	ω^3_{4a}	0.69	0.45	0.56
4	ω'^4_{3a}	0.63	0.61	0.60
	ω'^4_{4a}	0.67	0.55	0.67
5	ω'^5_{3a}	0.67	0.61	0.45
	ω'^5_{4a}	0.79	0.54	0.60
6	ω^6_{3a}	0.68	0.48	0.49
	ω^6_{4a}	0.69	0.44	0.42
7	ω'_{2a}	0.93	0.47	0.47
1	ω^1_{1b}	0.48	0.12	0.13
1′	$\omega^{1'}_{1b}$	0.48	0.42	0.41
2	ω'_{1b}	0.32	0.30	0.31
3	ω'^3_{3b}	0.51	0.51	0.58
	ω'^3_{4b}	0.70	0.48	0.43
4	ω^4_{3b}	0.68	0.49	0.49
	ω^4_{4b}	0.76	0.43	0.57
4′	$\omega^{4'}_{3b}$	0.69	0.60	0.52
	$\omega^{4'}_{4b}$	0.76	0.54	0.50
5	ω^5_{3b}	0.69	0.61	0.50
	ω^5_{4b}	0.76	0.41	0.43
6	ω'^6_{3b}	0.71	0.59	0.58
	ω'^6_{4b}	0.79	0.54	0.53
7	$\omega_{\mathbf{2b}}$	0.82	0.44	0.43

experiments for the Zr-Nb alloy.

The values of the binding energies in Table 3 are used in order to obtain the different pair concentrations. This is done with the help of expression (20) together with the values of the vacancy formation energies and entropies displayed in Table 2.

As we have mentioned earlier the migration energies E_m, are obtained with the Monomer method [9]. Table 4, reports the migration barriers calculated related to jumps in Fig. 1. For the different possible jumps involved in the 13-frequency model of Allnatt et al. we obtained the activation energy for jump within the basal plane and that between adjacent basal planes. Table 4 displays the migration energies obtained with classical MS, as well as, with quantum DFT for LDA and GGA approximations. In some cases the jump energies involved to obtain a given frequency (say for example ω'_{3a}) are not strictly equivalent. In that case the jump frequencies are distinguished with a superscript number denoting the final state of the vacancy (as described in Figs. 1 and 3).

Results of migration barriers, E_m, in Table 4, for $\alpha Zr-Nb$ alloy, with MS and DFT calculations reveal that the influence of *Nb* is relevant in *Zr* self-migration in comparison with results in pure αZr (first two rows of Table 4). Comparing the values of ω'_0 and ω_0 for pure *Zr* migration with ω'_{2a} and ω_{2b} for *Nb* migration in the alloy we can see that, according to MS results, the solute migrates in the axial/basal plane faster than pure *Zr*. While results from DFT-LDA and DFT-GGA show the opposite. This fact has important implications on the diffusion coefficient, as will be seen later.

In order to compute the mean jump frequencies ω_i and ω'_i we use expression (22) and (23) with the migration barriers, E^m_α summarized in Table 4, together with the migration entropies S^m_α for axial/basal planes displayed in Table 2. Note that, however S^m_α are different for each frequency, we have adopted for our calculations the constant value of S^m_α obtained from the pure αZr case.

In Table 5 we display MS migrations barrier calculations for more distant neighbors sites, this jumps are not involved in Ghate's nor Allnat's models. We can observe from results in Table 5 that in the alloy, classical calculations reveal an important deviation of the mean jump frequencies, due to *Nb* impurities, in comparison with the jump frequencies in pure αZr.

Once the jump frequencies needed for the multi-frequency models have been computed, the diffusion parameters can be calculated. Also, experimental results are available for the analysis of the diffusion in the anisotropic structure of αZr.

Table 5
More distant migration barriers in Zr-Nb from **MS** calculations.

n	a) 3^{rd}	b) 4^{th}
1	0.50	0.57
2	0.59	0.62
3	0.61	0.79
4	0.63	
5	0.69	
6	0.71	

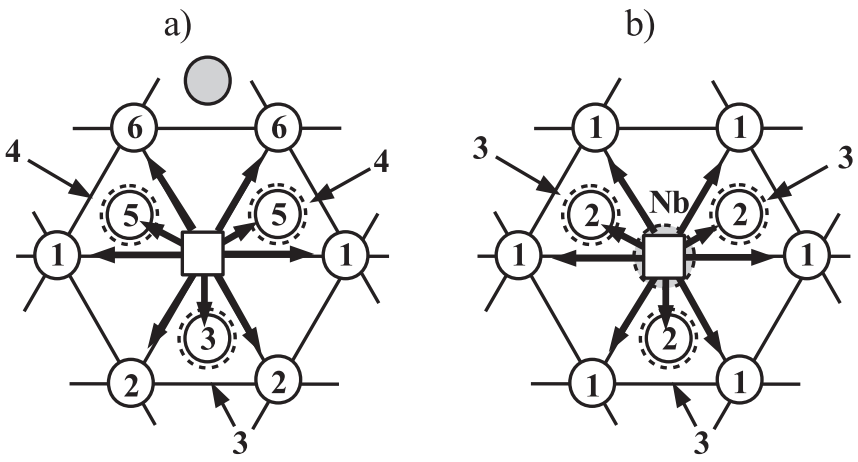

Fig. 3. Mean jump frequencies for *Nb* a) 3^{rd}, and b) 4^{th} neighbor to the Vacancy (open square). White circles correspond to the site reached by the vacancy after jump. Numbers are related to index **n** in Table 5.

As we can observe in Table 4, in some cases the jump energies involved to obtain a given frequency are not exactly equivalent. Hence in that cases, we define effective frequencies determined by an average weighted by the number of path-ways to each nearest-neighbor distance as shown below,

$$4\omega_{3a}^{\star} = 2\omega_{3a}^{(3)} + 2\omega_{3a}^{(6)}\,, \tag{64}$$

$$3\omega_{3a}^{\star\prime} = \omega_{3a}^{\prime(4)} + 2\omega_{3a}^{\prime(5)}\,, \tag{65}$$

$$2\omega_{1b}^{\star} = \omega_{1b}^{(1)} + \omega_{1b}^{(1')}, \tag{66}$$

$$3\omega_{3b}^{\star} = \omega_{3b}^{(4)} + \omega_{3b}^{(4')} + \omega_{3b}^{(5)}, \tag{67}$$

$$4\omega_{3b}^{\star\prime} = 2\omega_{3b}^{\prime(3)} + 2\omega_{3b}^{\prime(6)}\,. \tag{68}$$

5.1. Results with Ghate's 8-frequency model

First, we summarize the here performed calculations of the full set of the diffusion parameters, using Ghate's 8-frequency model [1] for h.c.p. lattices. Namely we have determined correlation factors for *Nb* solute, as well as, the tracer self- and solute diffusion coefficients both in the axial and basal plane.

In order to obtain the self diffusion coefficients in the axial and basal plane we employ respectively Eqs. (28) and (29). As in Ref. [23] we assume a constant value $f = 0.781$ for the partial correlation factors f_A^z, f_A^x and f_{Ab}. For the study of *Nb* diffusion in *Zr*, the tracer solute correlation factors involved in the diffusion equations are calculated from Eqs. (32)–(34).

Fig. 4 displays the correlation factors f_S^z, f_S^x and f_{Ab}, (respectively from Eqs. (32)–(34), as a function of temperature using MS, DFT-LDA and DFT-GGA calculations. All these magnitudes were plotted as functions of the inverse of the absolute temperature $(10^3/T)$. The jump rates needed to calculate the correlation and collective correlation factors have been obtained from Table 4.

With the correlation factors, the solute diffusion coefficients in axial and basal planes are then obtained from Eqs. (30) and (31) respectively. Fig. 5, summarizes our results of the tracer self- and solute diffusion coefficients using the Ghate's model with MS as well as DFT-LDA and DFT-GGA calculations.

In order to check the validity of the theory and numerical calculations, experimental results of self diffusion in pure αZr structure and of the *Nb* diffusion in the alloy, are also plotted in Fig. 5.

Horvath et al. [43] and Lubbehusen et al. [39] performed self diffusion measurements in single crystal αZr. Their results differ from more recent measurements by Hood et al. [42] for *Fe* free αZr. The reason for this discrepancy has been devised in Ref. [37] were, as much as, 50*ppm* of *Fe* impurities implies in differences of one order of magnitude for self-diffusion coefficients. Also, the *Nb* contain of the alloy implies in an enhancement of the self-diffusion coefficient.

Hood et al. [42] have estimated that according with the *Nb* concentration, C_{Nb}, the self-diffusion in the $\alpha Zr - Nb$ alloy can be described by,

$$D(Zr,A) = D(Zr,0) + 2C_{Nb}D(Nb), \tag{69}$$

where $D(Zr,0)$ is the self diffusion coefficient in pure αZr and $D(Nb)$ is the *Nb* diffusion coefficient in the alloy. They have obtained experimentally in Ref. [42] that for pure *Zr*:

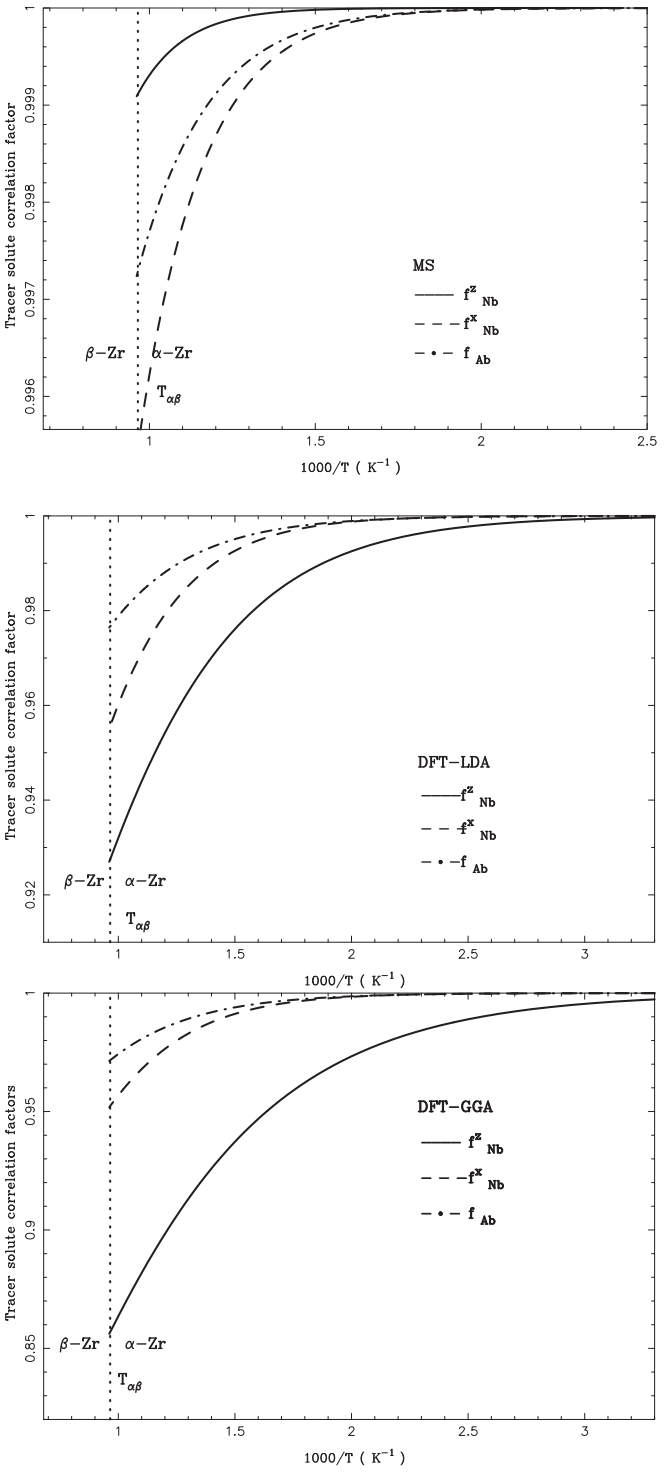

Fig. 4. The tracer correlation factors in Ghate's 8-frequency model [1]. a) MS, b) LDA and, c) GGA approximations.

$$D(Zr,0) = 1.66 \times 10^{-4}\exp(-3.20eV/k_BT)\; m^2/s, \tag{70}$$

and the *Nb* solute diffusion coefficient [40] is

$$D(Nb) = 1.88 \times 10^{-4}\exp(-2.69eV/k_BT)\; m^2/s. \tag{71}$$

In Fig. 5 we have plotted, with black stars and open circles, the

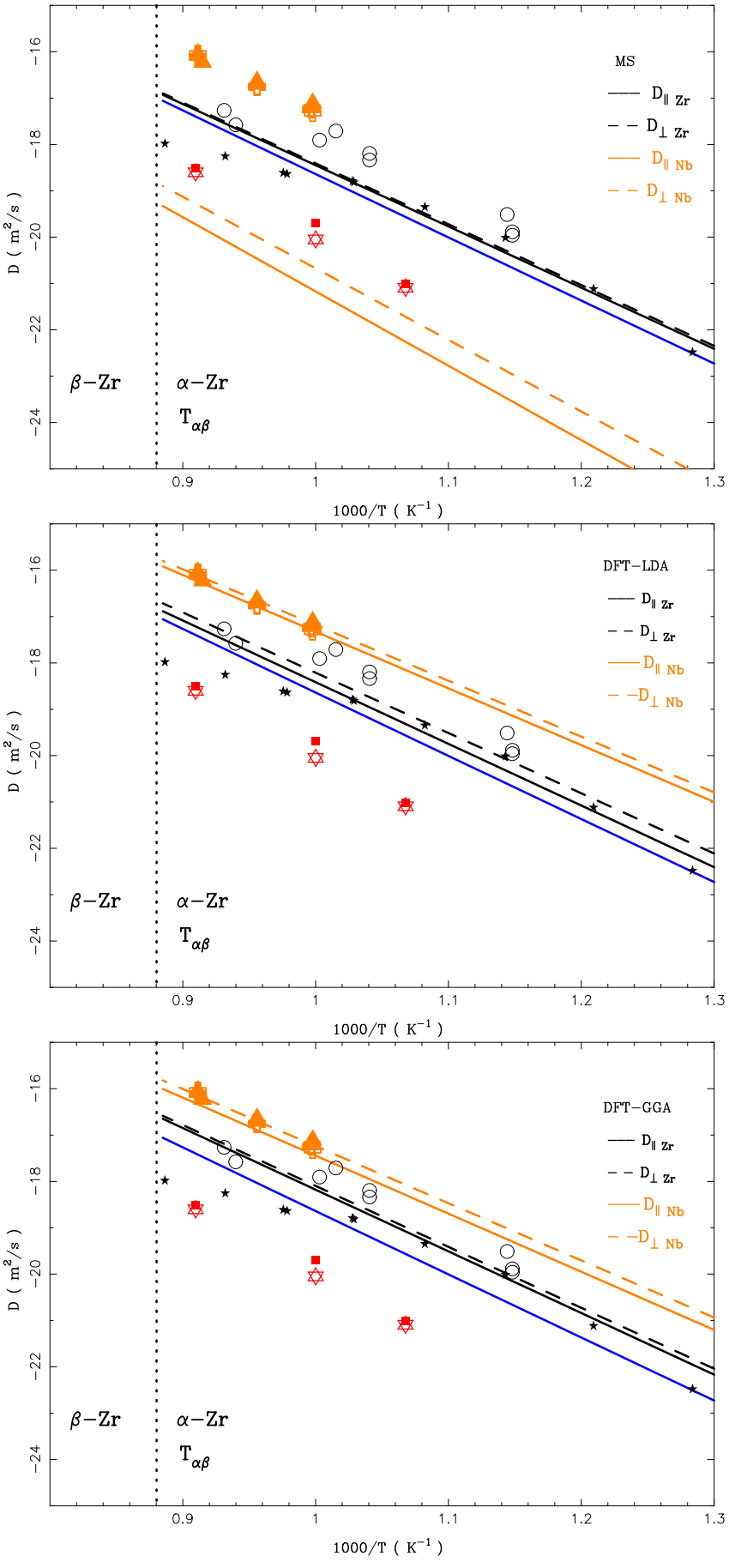
MS
$D_{\parallel Zr}$
$D_{\perp Zr}$
$D_{\parallel Nb}$
$D_{\perp Nb}$
β−Zr
α−Zr
$T_{\alpha\beta}$
D (m^2/s)
1000/T (K^{-1})
DFT−LDA
DFT−GGA

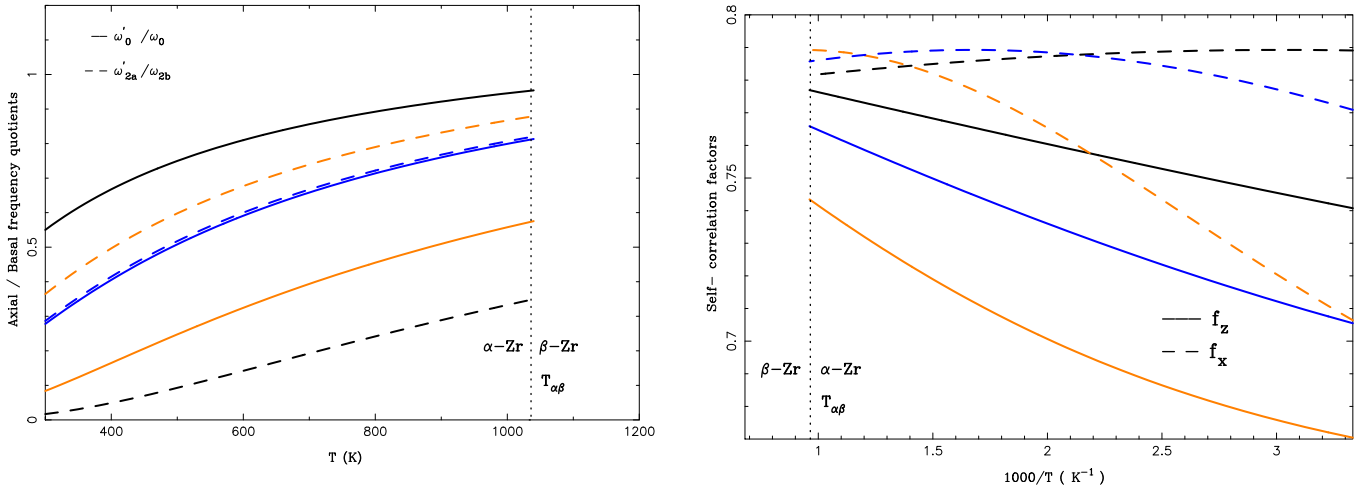

Fig. 6. Solid lines stand for axial and dashed lines for basal magnitudes. MS (in black), LDA (in orange) and GGA (in blue) calculations. Left panel: temperature dependence of axial/basal frequency ratios. Right panel: temperature dependence of the tracer self-correlation factors from Eqs. (40) and (41). (For interpretation of the references to colour in this figure legend, the reader is referred to the web version of this article.)

experimental data for *Zr* self diffusion coefficients from Refs. [43] and [39], respectively. Also, the experimental data for self-diffusion from Ref. [42] are plotted with red stars and full squares. Meanwhile, self-diffusion coefficient for the alloy, calculated from equation (69) is shown with blue solid line, in Fig. 5. Also, the experimental data for the *Nb* tracer diffusion [40] are plotted, in Fig. 5, with orange crosses and triangles.

Fig. 5 shows that, although the three *Zr* self-diffusion coefficients (black lines), calculated from expressions (28) and (29) with all correlation factors $f = 0.78$, for MS, LDA and GGA, give different results they all are in an interval of agreement with the experimental data in Refs. [43] (black stars) and [39] (black circles). Also, the mentioned calculated diffusion coefficients are close to the blue line describing the tracer self-diffusion in the alloy. However, calculations using constant correlation factors $f = 0.78$ describe the self diffusion in pure αZr, not in the alloy, hence we would have expect for them a better agreement with experimental data from Ref. [42] (red symbols).

On the other hand, Fig. 5 shows that the solute trace diffusion coefficient of *Nb*, obtained from MS calculations, is lower than that of *Zr* for the whole range of temperature. This result is contrary to the experimental data of *Nb* diffusion in α *Zr* in Ref. [40] (orange symbols in Fig. 5). This fact is due to the higher values, obtained with MS calculations, of ω'_{2a} and ω_{2b} for *Nb* migration in the alloy in comparison with ω'_0 and ω_0 for pure *Zr* migration. Consistently with a strong repulsive binding between solute and vacancy. We believe that this issue, with our MS calculations, denotes a lack of reliability of the pseudo potential used for the *Nb*. It would be then useful for an update of the pseudo potential in order to better describe the *Nb* interaction.

Instead, for the rest of the calculations, DFT-LDA and DFT-GGA, the opposite behavior ($D^{\star}_{Nb} > D^{\star}_{Zr}$) is observed for diffusion in both, parallel and perpendicular to the *z* axis. Also, the agreement between results from DFT-LDA and DFT-GGA calculations in comparison with the experimental data of Ref. [40], orange symbols in Fig. 5, is noticeable.

Therefore, we must conclude that both, DFT-LDA and DFT-GGA approximations, accurately describe the experimental data for *Nb* solute diffusion in the alloy.

5.2. Results with the 13-frequency model by Allnatt ***et al*** [2]

5.2.1. Isotope limit case: self-diffusion in pure αZr

The isotope limit is defined as the case where the solute, *S*, is an isotope of the solvent, *A*, so that all exchange frequencies are either ω_0 or ω'_0. In this case, the correlation factor, *f*, varies with the frequency ratio $x = \omega_0/\omega'_0$ as in Eqs. (40) and (41). Fig. 6 shows the frequency ratio for the pure metal as a function of the temperature, as well as, the correlation factors obtained through Eqs. (40) and (41).

Our results in Fig. 6 (right panel) show that, the tracer correlation factors deviate from a constant value of $f = 0.78$ with the inverse of the temperature for both, axial and basal directions.

Self-diffusion data in αZr are shown in Fig. 7, the calculations have been performed using Eqs. (42) and (43), together with the correlation factors in (40) and (41), for diffusion in the axial and basal plane, respectively. As before, we corroborate our calculations with available experimental data of self-diffusion. From Fig. 7, we can observe that, similarly to the results obtained with $f = 0.78$, depicted in Fig. 5, the isotopic limit of self diffusion coefficients, calculated with MS, LDA or GGA, give results that are all in an interval of agreement with the experimental data in Refs. [43] (black stars) and [39] (black circles). Again, the calculations do not agree with experimental data obtained by Hood et al. [42] (red symbols).

In the right panel of Fig. 7 we display the ratio between the self-diffusion coefficients $D^{\star}_{\parallel}/D^{\star}_{\perp}$ that takes values between 0.92 and 0.85, 0.63–0.46 and 0.84–0.72 *vs* $1/T$, respectively for MS, LDA and GGA calculations. This shows the anisotropy of the diffusion process.

The results here obtained for the isotopic limit of the formulation of Allnatt [2], coincide with those for the self-diffusion using expressions (28) and (29) with $f = 0.78$, displayed in Fig. 4, in black

Fig. 5. Tracer self- and solute diffusion coefficients using the 8-frequency model. Solid and dashed lines, for basal and axial diffusions respectively. Black lines: self-diffusion calculations. Experimental data for *Zr* self diffusion: black stars [43], circles [39]; red stars and squares [42]. Blue line: self diffusion in the alloy from Eq. (69). Orange lines: *Nb* diffusion calculations. Orange crosses and triangles: experimental data for *Nb* diffusion [40]. From top to bottom, results obtained with MS, LDA and GGA, calculations. (For interpretation of the references to colour in this figure legend, the reader is referred to the web version of this article.)

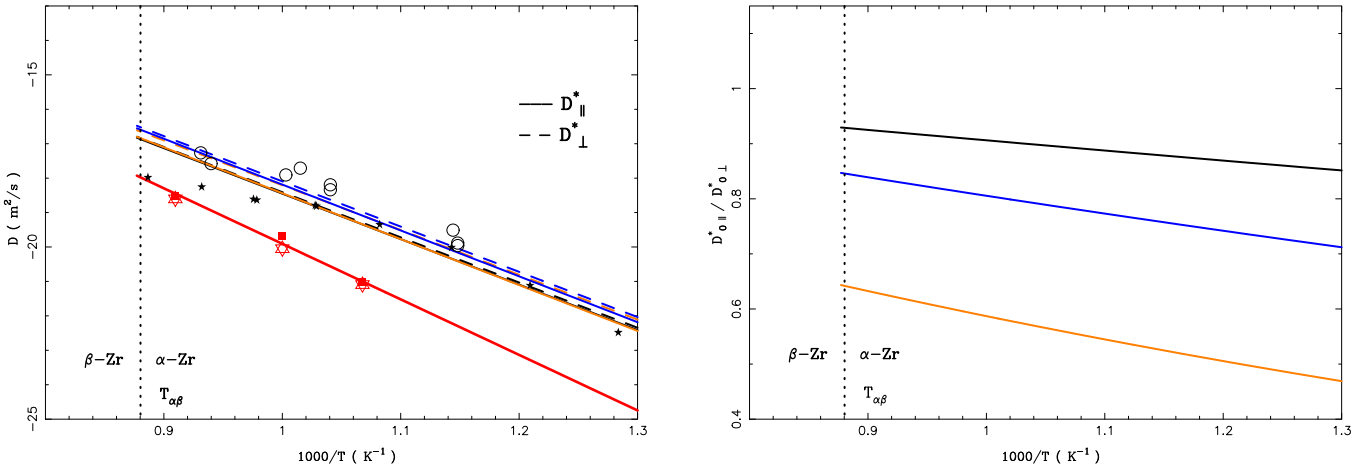

Fig. 7. Isotope limit case: MS (in black), LDA (in orange) and GGA (in blue) calculations. Right panel: self-diffusion coefficients, solid lines stand for axial and dashed lines for basal magnitudes. Experimental data for *Zr* self diffusion in black stars [43], circles [39]; red stars and squares [42]. Left panel: anisotropy ratio $D^{\star}_{\parallel}/D^{\star}_{\perp}$. (For interpretation of the references to colour in this figure legend, the reader is referred to the web version of this article.)

solid and dashed lines, for the three approximations used here, i.e., MS, DFT-LDA and DFT-GGA.

In this section, we verify that the LDA approximation describes quite well the experimental data, and shows that the diffusion coefficients in the axial and basal planes verify the relation $D^{\star}_{\perp} \simeq 2D^{\star}_{\parallel}$ (in agreement with results for pure αZr in Ref. [37]). While for MS and DFT-GGA calculations, the anisotropy is bigger.

5.2.2. *Tight-binding approximation: diffusion in diluted αZr – Nb alloy*

In the Allnatt's et al. model [2] the tracer self- and solute diffusion coefficients in the Axial/Basal plane are calculated respectively from Eqs. (54), (56) and (57)–(55). Introducing the effective frequencies (64–68), the tracer solute correlation factors involved in the axial and basal directions are calculated from Eqs. 46 and 48. Then, the two collective correlation factors f^{i}_{AA} and $f^{(S)i}_{AS}$ (with $i = x, z$), are respectively calculated from Eqs. (44), (45) and (48). In Figs. 8 and 9, we plot the solute correlation factors, f^{i}_{S} (with $i = x, z$), as well as, the two collective correlation factors f^{i}_{AA} and $f^{(S)i}_{AS}$ (with $i = x, z$). Note that we assume, as in Ref. [2], that $f^{i}_{SS} = f^{i}_{S}$ and $f^{i}_{A} = f^{i}_{AA}$ (with $i = z, x$). All these magnitudes were plotted as functions of the inverse of the absolute temperature ($10^3/T$).

Fig. 8 summarizes the solute correlation factor calculations, f^{i}_{S}. It can be observed that f^{i}_{S}, has a larger variation range in the temperature range of the h.c.p. phase, when the calculations are performed with the DFT-GGA approach (solid and dashed lines in blue). While classical calculations and quantum ones with DFT-LDA, show that $f^{x,z}_{S}$ is much closer to one. Note that, has was seen in equation (48), $f^{i}_{AS} = -2f^{i}_{S}$, so that, $f^{i}_{AS} \simeq 2$, for MS as well as for LDA

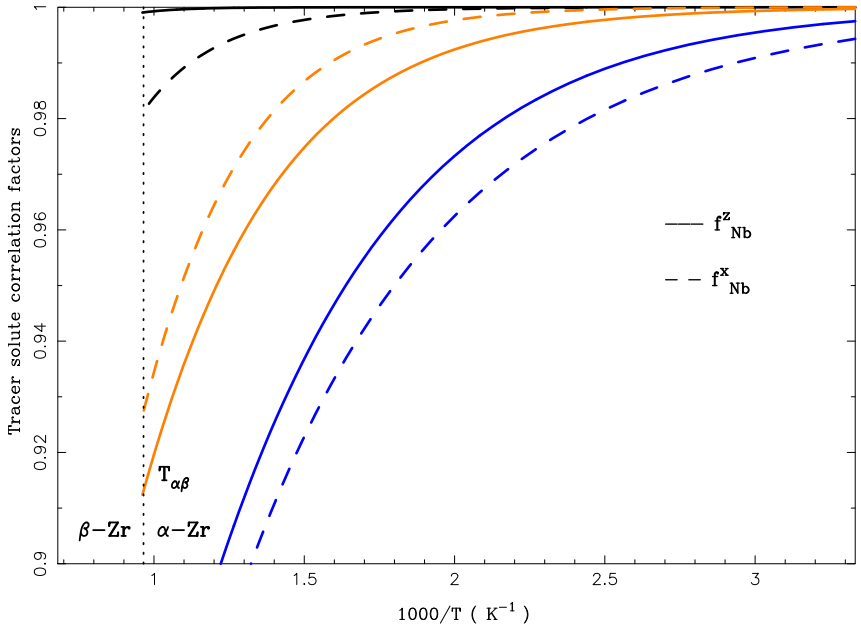

Fig. 8. Correlation factors as functions of the inverse of the temperature for the case of vacancy-solute tight-binding (no free vacancies). Solid lines stand for axial and dashed lines for basal magnitudes. MS (in black), LDA (in orange) and GGA (in blue) calculations. (For interpretation of the references to colour in this figure legend, the reader is referred to the web version of this article.)

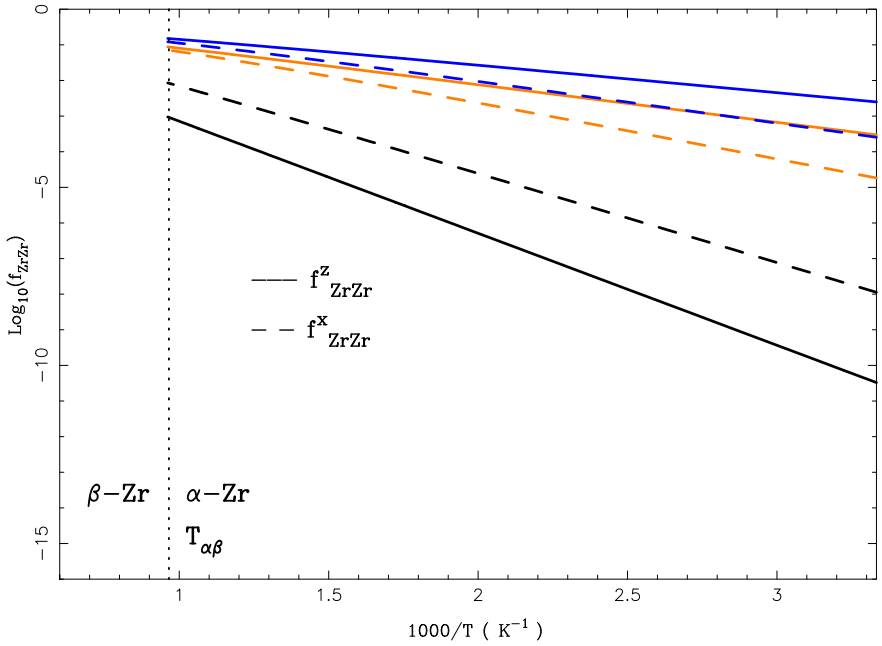

Fig. 9. Temperature dependence of the collective correlation factors $f^{z,x}_{ZrZr}$. Solid lines stand for axial and dashed lines for basal magnitudes. MS (in black), LDA (in orange) and GGA (in blue) calculations. (For interpretation of the references to colour in this figure legend, the reader is referred to the web version of this article.)

and GGA approximations.

Fig. 9 shows the remaining sets of collective correlation factors, where both solvent correlation factors, f^i_{AA} (with $i = x, z$), follow an Arrhenius behavior.

Once the correlation factors have been obtained, the tracer solute diffusion coefficients are evaluated from Eqs. (54) and (55), respectively for axial and basal plane. Also, the self-diffusion coefficients in axial/basal directions are obtained using Eqs. (56) and (57).

Fig. 10 shows the tracer self-diffusion and the tracer solute diffusion coefficients, calculated with the three different approaches. Solid and dashed lines refer to diffusion in the axial and basal plane, respectively. In Fig. 10, black and orange colors refer to solvent and solute diffusivities respectively.

It must be noted that tight binding limit approximation, here used for the 13 frequency model, is only valid for an attractive solute-vacancy binding. As is seen in Table 3 this condition is not reached with MS calculations, where the interaction between solute and vacancy is strongly repulsive i.e. they have positives binding energies. Indeed, in Fig. 10 we can appreciate the discrepancy between diffusion coefficients calculated with MS and experimental data. As we have already mentioned, this fact is an issue of the empirical pseudo potential used by MS calculations. The development of a more reliable pseudo potential for the *Nb* is required in order to perform MS calculations accurately.

Also, we can observe that for the *Nb* solute diffusion, the results obtained with the 13-frequencies model by Allnat et al. [2] in the tight-binding limit, shown with orange lines in Fig. 10, are very similar to the ones calculated with the Ghate's 8-frequencies model [1], shown in Fig. 5. This similarity is valid for the three calculation methods MS, LDA and GGA. Although, the results obtained with MS calculations are not reliable, as we have already discuss.

On the other hand, the comparison of the self-diffusion behavior shown with black lines in Figs. 10 and 5 are different. In this respect, for the case of solvent diffusion in the alloy, only the 13-frequency model, by Allnatt et al. [2] takes into account the presence of *Nb* atoms for the *Zr* migration. As we have previously mentioned, black lines in Fig. 5 describe the self-diffusion in pure *Zr* and hence must be compared with the isotopic limit case shown in Fig. 7. For the case of *Zr* diffusion in the alloy, the results obtained with both LDA and GGA, (black lines in Fig. 10) are in good agreement with experimental data in Ref. [43] (black stars) and [39] (black circles).

Also, it is important to remark from Fig. 10 the agreement between *Zr* diffusion behavior obtained from GGA calculations with the prediction in equation (69) for the diffusion in the alloy made by Hood et al. [42] (blue line).

As mentioned above, our calculations with the 13-frequency model were performed in tight-binding limit. This applies only if the binding between solute and vacancy is strongly attractive so that there are no vacancies or solute atoms unpaired. There is then no possibility of dissociation of pairs, and diffusion expressions do not depend on the frequencies ω_3 labeled frequencies. Thus, the model only depends on 8-frequencies, which are different from those employed by Ghate's model. Our calculations show that despite the attractive interaction between solute and vacancy being mild, the results obtained for the diffusion employing the tight-binding model are in very good agreement with the experimental data.

In addition, for the LDA and GGA cases, where the lattice ratio c/a is close to the ideal ($c/a \simeq 1.63$), we have studied the 5-frequencies limit for the correlation factors [2], described earlier. In Fig. 11 we display the diffusion coefficients obtained by using the 5-frequencies correlation factors from Eqs. (58) and (59) for the z axis inserted in expressions (54) and (56) respectively. While for the *x*-axis correlation factors (60) and (61) are respectively inserted in Eqs. (55) and (57). In that case the frequencies ω_1 and ω_2 used in the model are obtained as average frequencies,

$$\omega_1 = \frac{1}{4}\left(\omega_{1a} + \omega_{1b} + \omega'_{1a} + \omega'_{1b}\right),$$

and

$$\omega_2 = \frac{1}{2}\left(\omega_{2b} + \omega'_{2a}\right)$$

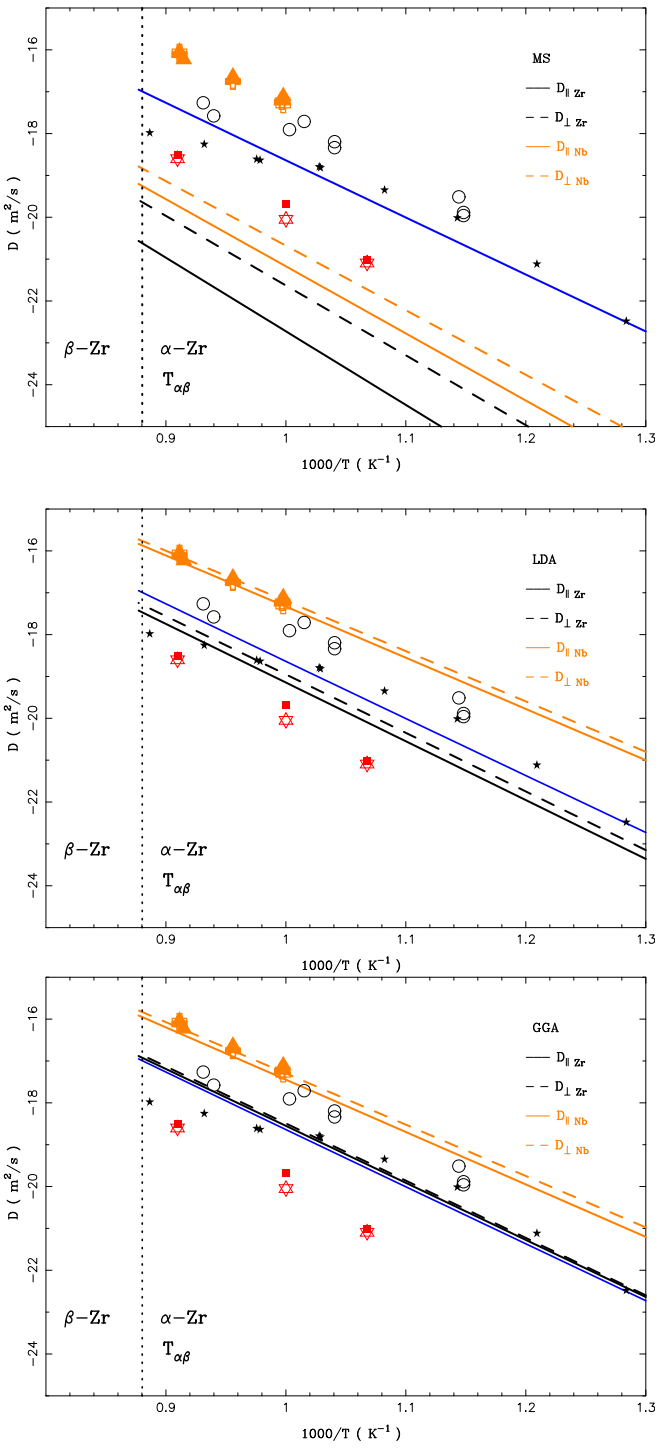

Fig. 10. Tracer self- and solute diffusion coefficients using the 13-frequency model. Solid and dashed lines, for basal and axial diffusions respectively. Black lines: self-diffusion calculations. Experimental data for *Zr* self diffusion: black stars [43], circles [39]; red stars and squares [42]. Blue line: self diffusion in the alloy from Eq. (69). Orange lines: *Nb* diffusion calculations. Orange crosses and triangles: experimental data for *Nb* diffusion [40]. From top to bottom, results obtained from MS, LDA and GGA, calculations.

It can be observed, comparing Fig. 11 with Fig. 10, that the results obtained with the 5-frequency limit are very similar to those obtained with 13-frequency model in the tight-binding limit. Hence, the 5-frequency model in the tight-binding approximation is enough in order to describe the diffusion process in diluted $\alpha Zr - Nb$ alloy. In this case, as mentioned earlier, the diffusion coefficients only depend on 3 frequencies, namely ω_0, ω_1 and ω_2.

6. Concluding remarks

In this paper, we have numerically studied diffusion for the anisotropic three-dimensional h.c.p. structure of αZr including substitutional *Nb* foreign atoms, as well as, a single vacancy.

Two models of atomic diffusion in h.c.p have been studied, namely Ghate's model [1] involving eight frequencies and the 13 frequency model [2] recently developed by Allnatt, Belova and Murch [2]. This last model is here applied for the first time to a particular alloy.

We have reviewed both diffusion models and present the general mechanism based on non-equilibrium thermodynamics and the kinetic theory, to describe the diffusion behavior in h.c.p diluted alloys. Non equilibrium thermodynamic, through the flux equations, relates the diffusion coefficients with the Onsager tensor, while the Kinetic Theory relates the Onsager coefficients in terms of microscopical magnitudes. In this way we are able to write expressions for the diffusion coefficients only in terms of microscopic magnitudes, i.e. the jump frequencies.

In this respect, the jump frequencies have been calculated from the migration barriers which are obtained with an economic static molecular techniques namely the monomer method, that searches saddle configurations efficiently in MS and, more even, in ab-initio calculations, reducing at a half the force calculations.

We have exemplified our calculations for the particular cases of diluted Zr-Nb h.c.p. binary alloy. Migration energies were obtained with three different approaches. With potential semi empirical and classical MS besides using ab-initio quantum calculations in two different approximations for DFT, namely LDA and GGA.

Our results show that for self-diffusion of pure αZr, either with a constant correlation factor $f = 0.78$ or with the expressions of Alnatt et al. [2] for the isotopic case, the results are very similar and the calculations obtained with both three MS, LDA and GGA techniques are consistent with experimental data. Although there seems to be no clear consensus on the latter.

With respect to the solvent diffusion of *Zr* in the alloy, only the 13 frequencies model is applicable. In this case, both LDA and GGA give very good results consistent with predictions based on experimental data.

Regarding the diffusion of *Nb* in the alloy, the comparison of the results of both models 8 and 13 frequencies are very similar for the respective calculations. Note that the MS calculations are far away from the experimental results (in both models). In fact the energies of migration and binding give implausible results. We believe that this issue, with our MS calculations, denotes a lack of reliability of the pseudo potential used for *Nb*. It urges then for a new pseudo potential in order to better describe the *Nb* interaction. On the other hand, the results with both DFT approximations, LDA as well as GGA, show a very good agreement with the experimental results.

It is also noteworthy that the 5 frequencies limit approximation and the 13 frequencies model in the tight binding approximation, gives very similar results that are also in agreement with experimental data. Thus if the lattice has a c/a ratio close to the ideal, the use of the 5 frequencies approximation is enough to describe the main features of the diffusion process. Therefore, we can say that this simple model, that does not take into account either the dissociation of pairs or anisotropy in the jump frequencies, is

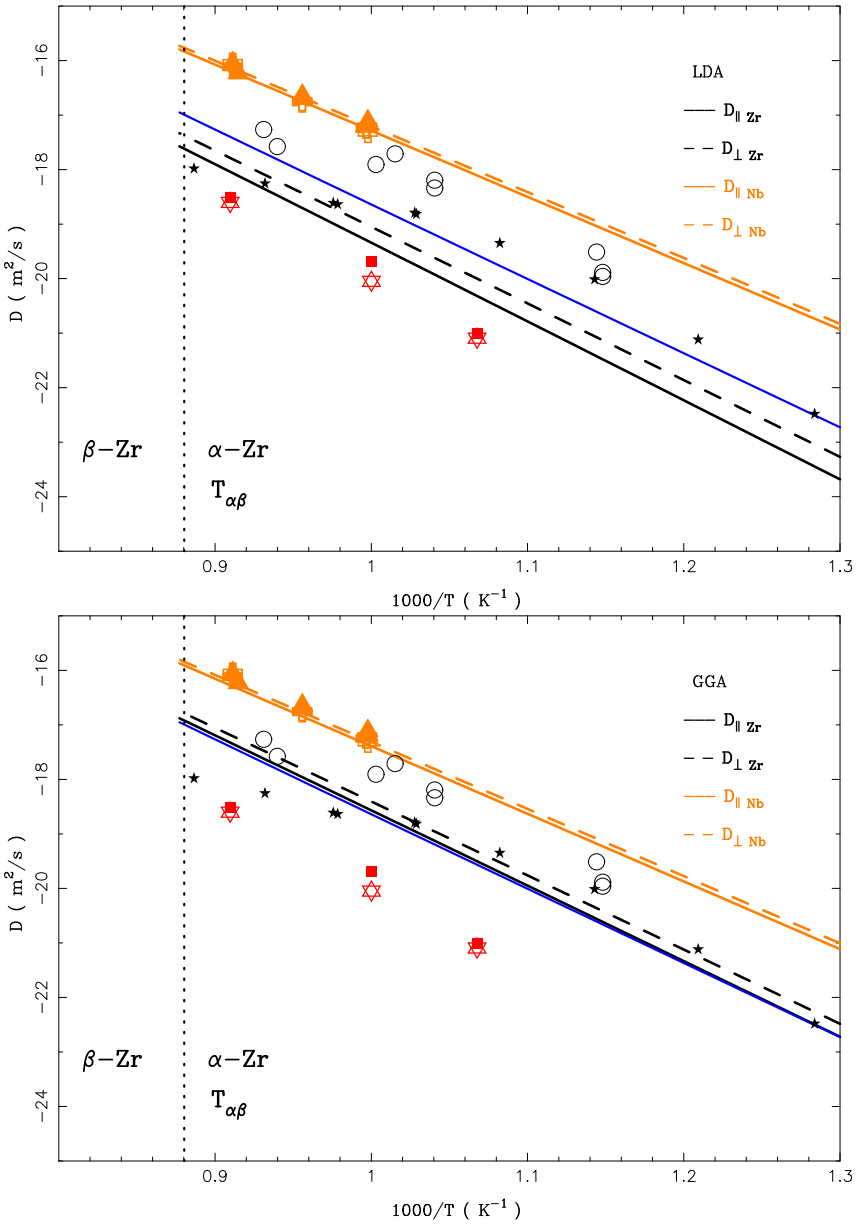

Fig. 11. Tracer self- and solute diffusion coefficient, using the 5-frequency limit for the h.c.p. lattice. The colors and patterns, as in Fig. 10.

sufficient to describe the anisotropic diffusion process in this h.c.p. alloy. In this case, the diffusion coefficients only depend on 3 frequencies.

We are performing similar calculations for the treatment of diluted $\alpha Zr - Fe$ alloy, in which the attractive binding between vacancy and solute *Fe* is strong.

Acknowledgements

This work was partially financed by CONICET PIP-00965/2010.

References

[1] P. Ghate, Phys. Rev. 133 (1964) A1167.
[2] A.R. Allnatt, I.V. Belova, G.E. Murch, Philos. Mag. 94 (22) (2014) 2487–2504.
[3] V.P. Ramunni, Comput. Mater. Sci. 93 (2014) 112.
[4] S. Choudhury, L. Barnard, J.D. Tucker, T.R. Allen, B.D. Wirth, M. Asta, D. Morgan, J. Nucl. Mater 411 (2011) 1.
[5] A.L. Claire, J. Nucl. Mater 69–70 (1978) 70.
[6] Y. Serruys, G. Brebec, Philos. Mag. A 46 (1982) 661.
[7] A.R. Allnat, J. Phys. C. Solid State Phys. 14 (1981) 5453–5466.
[8] A.R. Allnat, J. Phys. C. Solid State Phys. 14 (1981) 5467–5477.
[9] V.P. Ramunni, M.A. Alurralde, R.C. Pasianot, Phys. Rev. B 74 (054113) (2006).
[10] J.D. Tucker, et al., J. Nucl. Mater 405 (2010) 216.
[11] M. Mantina, et al., Acta Mater. 57 (2009) 4102.
[12] S. Huang, et al., Acta Mater. 58 (2010) 1982.
[13] V.P. Ramunni, A.M.F. Rivas, Mater. Chem. Phys. 162 (2015) 659–670.
[14] A.P. Batra, Phys. Rev. 159 (1967) 487.
[15] L. Huber, I. Elfimov, J. Rottler, M. Militzer, Pys. Rev. B 85 (2012) 144301.
[16] Bi-Cheng Zhou, Shun-Li Shang, Wang Yi, Zi-Kui Liu, Diffusion coefficients of alloying elements in dilute Mg alloys: a comprehensive first-principles study, Acta Mater 103 (2016) 573–586.
[17] G.H. Vineyard, J. Phys. Chem. Solids 3 (1957) 121.
[18] A.R. Allnat, A.B. Lidiard, Atomic Transport in Solids, Cambridge University Press, 2003.
[19] R.E. Howard, Phys. Rev. 144 (1966) 650.
[20] G.E. Murch, Z. Qin, Defect Diffus. Forum 109 (1994) 1–18.
[21] G.E. Murch, I.V. Belova, Diffus. Fundam. 2 (2005), 8.1-8.13.
[22] N.I. Peterson, J. Nucl. Mater. 69 (1978) 3–37.
[23] R.C. Pasianot, R.A. Pérez, V.P. Ramunni, M. Weissmann, J. Nucl. Mater. 392 (1) (2009) 100–104.
[24] J.M. Soler, E. Artacho, J.D. Gale, A. Garcia, J. Junquera, P. Ordejón, D. Sanchez-

Portal, J. Phys. Cond. Matter 14 (2002) 2745.
[26] G. Verité, F.W. Willaime, C.C. Fu, Solid State Phenom. 129 (2007) 75.
[27] R.C. Pasianot, A.M. Monti, J. Nucl. Mater. 264 (1999) 198–205.
[28] J.R. Fernández, A.M. Monti, y G. Simonelli, Anales AFA 19, Salta, 2007, pp. 136–140.
[29] G. Henkelman, H. Jónsson, J. Chem. Phys. 111 (2002) 15. Surfaces, Interfaces, and Materials.
[30] V.O. Kharchenko, D.O. Kharchenko, Condens. Matter Phys. 16 (1) (2013) 1–8, 13801.
[31] C. Domain, J. Nucl. Mater 351 (2006) 1.
[33] D. Ruiz, L.M. Gribaudo, A.M. Monti, Mater. Res. 8 (4) (2005) 431–434.
[34] R.C. Pasianot, R.A. Pérez, Phys. B 407 (2012) 3298–3300.
[35] G. Hood, J. Nucl. Mat. 139 (1986) 179.
[36] X.K. Xin, W.S. Lai, B.X. Liu, J. Nucl. Mater 393 (1) (2009) 197–202.
[37] G.M. Hood, R.J. Schultz, N. Matsuura, J. Nucl. Mater 226 (1995) 260.
[39] M. Lubbehusen, K. Vieregge, G.M. Hood, H. Mehrer, C. Herzig, J. Nucl. Mater 182 (1991) 164.
[40] G.M. Hood, H. Zou, R.J. Schultz, N. Matsuura, A.J. Roy, J.A. Jackman, Defect diff. Forum 143–147 (1997) 55–60.
[42] G.M. Hood, H. Zou, R.J. Schultz, N. Matsuura, A.J. Roy, J.A. Jackman, Defect diff. Forum 143–147 (1997) 49.
[43] J. Horváth, F. Dyment, H. Meherer, J. Nucl. Mater 126 (1984) 206.